Pergamon

Geochimica et Cosmochimica Acta, Vol. 67, No. 19, pp. 3687–3715, 2003

0016-7037/03 $30.00 + .00

doi:10.1016/S0016-7037(03)00132-7

A lead isotope method for the accurate dating of disturbed geologic systems: Numerical demonstrations, some applications and implications

FOUAD TERA*

Department of Terrestrial Magnetism, Carnegie Institution of Washington, 5241 Broad Branch Rd, NW, Washington, DC 20015, USA

(*Received December* 26, 2000; *accepted in revised form December* 29, 2002)

Abstract—Lead isotopes are compared in two equivalent diagrams. With a range in U/Pb, a closed system that evolved its radiogenic Pb in a single stage yields data that define a line of exactly the same age in the two presentations. This strict reproducibility (within ± a few 10^6 yr, at most) is the crux of the concept of *Pb-isotope synchronism*. In contrast, an open system produces data that disperse variably in the two diagrams, yielding ages which are often different by $\gg 10^7$ yr. However, because an age-calculation reconciles uncertainty in the age with the degree of dispersion in the data, a highly disturbed system yields false ages (from both diagrams), which nevertheless overlap within the calculated errors.

This dichotomy (tightly reproduced linearity of a closed system vs. loosely correlated dispersion of an open one) is exploited in a new procedure, termed *differential Pb correlation*. This procedure allows filtering the data, so that an imperfect isochron may be improved or an invisible one may be identified within a dispersion field.

Applying the synchronism method to the whole rock Pb isotopic data on the Amîtsoq gneisses results in their resolution into three synchronous lines, yielding the single-stage ages of 4.42, 3.74 and 3.45 Ga. In an attempt to reconcile this observation with geology, the mechanisms which may have produced these lines (*multi-stage lineation*) are explored. In addition, the possibility that the 4.42-Ga line is an actual isochron, and that vestiges of an ancient terrestrial crust of that age exist, are contemplated in some detail.

The utility of the method is further demonstrated by application to meteorites as well as terrestrial rocks. Isochrons of crustal rocks intersect with each other as subgroups in multiple places (that is, at multiple Pb isotope values). This indicates the apparent existence of terrestrial reservoirs distinct in isotopic composition from each other. One of these reservoirs, characterized by a low ($U/^{204}Pb$) = 4 may represent a depleted complement to the U-enriched source(s) of the ocean-island basalt (OIB). If so, then the so-called "Pb paradox" may no longer exist. *Copyright © 2003 Elsevier Ltd*

1. INTRODUCTION

In this report Pb isotopic data are presented and discussed, concurrently using two of the three types of diagrams: type I, $^{206}Pb/^{204}Pb$ vs. $^{207}Pb/^{204}Pb$; type II, $^{204}Pb/^{206}Pb$ vs. $^{207}Pb/^{206}Pb$; and type III, $^{204}Pb/^{207}Pb$ vs. $^{206}Pb/^{207}Pb$. Type I is the familiar conventional Pb-Pb diagram. Type II was introduced to facilitate presenting the highly radiogenic lunar data(Tera and Wasserburg, 1972a) and to allow direct correlation with a modified concordia diagram (Tera and Wasserburg, 1972b). Type III was included for the evaluation of terrestrial Pb contamination of meteoritic samples (Tera et al., 1997). Here the concurrent use of these diagrams is aimed at an aspect of the Pb systematics which hitherto has not been addressed; namely an inherent unique potential in the dual U-Pb clock to identify closed-system samples in the midst of open-system ones. Such potential derives from a consistent linear projection of closed-system data, and variably modulated dispersion of non-linear, open-system data, on the Pb-Pb diagrams.

A basic aspect of Pb isotope systematics is the ability to measure the age of a closed system (e.g., a rock) from the Pb isotopic composition of its components (e.g., the minerals) without having to determine the concentration of the parent isotopes, ^{235}U and ^{238}U. Applying the equation of radioactive decay, the age, τ is calculated from the relationship

$$*(^{207}Pb/^{206}Pb) = (1/137.88)\,[(e^{\lambda'\tau} - 1)/(e^{\lambda\tau} - 1)] \quad (1a)$$

Where $*(^{207}Pb/^{206}Pb)$ is the in-situ radiogenic daughter ratio, determined from either the slope or the intercept of the line (depending on the type of diagram used) defined by the data. λ' and λ are the decay constants of ^{235}U and ^{238}U, and 1/137.88 is the present-day ratio of the former isotope to the latter.

Although algebraically fully redundant, the three Pb isotope diagrams (mentioned above) are shown to yield three different $*(^{207}Pb/^{206}Pb)$ ages for an imperfect isochron. These ages, which are often grossly false, are by necessity always in agreement within errors. This non-diagnostic concurrence of ages from the three diagrams is inherent in the calculation of an isochron-age, where the magnitude of uncertainty in the age is in reality a quantification of the degree of dispersion of the data. What is diagnostic is the magnitude of disparity between the ages, which (as mentioned earlier) stems from the fact that the patterns of dispersion of open-systems are variably modulated in the three Pb diagrams. A procedure described in the text allows for the filtration of the modulated patterns, so that the line of the closed-system data may emerge. Thus the determination of an accurate isochron for a disturbed system may not only be possible, but also practical.

Synthetic as well as natural examples are given to show that under favorable, but not uncommon conditions, filtering of disturbed data leads to convergence of the ages from the diagrams on a *synchronous date* of the same numerical value and with uncertainty of no more than a few 10^6 yr.

* (tera@dtm.ciw.edu).

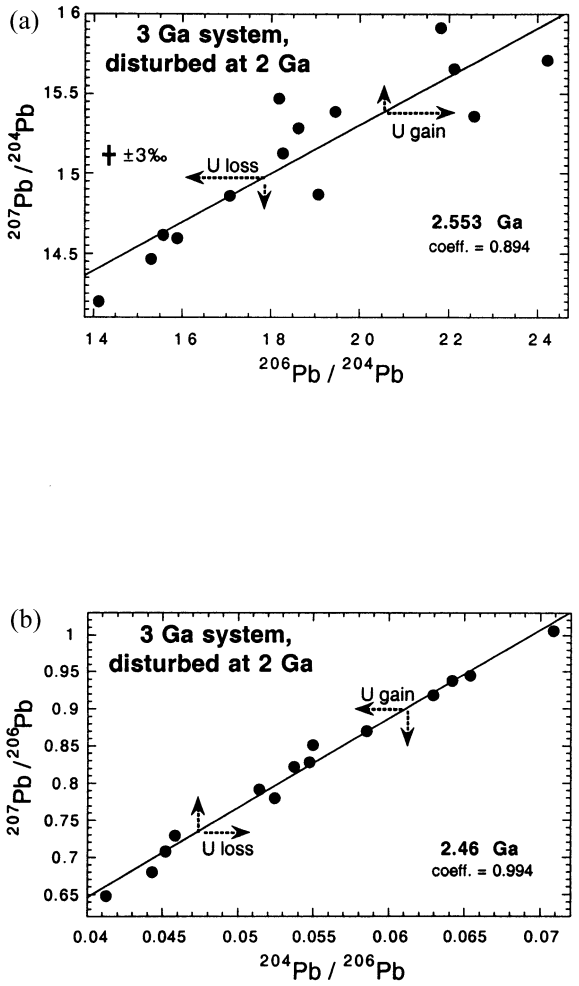

Fig. 1. (a) Synthetic Pb isotopic data (see Table 1) for a 3.000-Ga system which experienced a disturbance at 2.000 Ga when some of the components experienced U loss or gain (relative to Pb). The ranges of the trajectories of dispersion on the x-axis and y-axis of type I diagram (dashed arrows) are lopsided, resulting in a pronounced dispersion of disturbed samples. (b) Same data plotted on a type II diagram. Here the ranges of the trajectories of dispersion are comparable, leading to the suppression of shifts off a best-fit line, which yields a false age.

2. SYNCHRONISM

2.1. System-Errors

In Figures 1a and 1b are shown the data for a synthetic system which is 3.000 Ga old, and which was disturbed 2.000 Ga years ago when U and Pb were mobilized in some of the system's components. In other words the data shown (see Table 1), simulate a mix of rocks, some of which evolved their in-situ radiogenic Pb in a single stage (according to Eqn. 1b and 1c) and others, which evolved theirs in two stages (according to Eqn. 2a and 2b).

$$(^{206}Pb/^{204}Pb)_{Sam} = (^{206}Pb/^{204}Pb)_1 + \mu_2 \times (e^{\lambda\tau} - 1) \quad (1b)$$

$$(^{207}Pb/^{204}Pb)_{Sam} = (^{207}Pb/^{204}Pb)_1 + \mu_2' \times (e^{\lambda'\tau} - 1) \quad (1c)$$

$$(^{206}Pb/^{204}Pb)_{Sam} = (^{206}Pb/^{204}Pb)_1 + \mu_2 \times (e^{\lambda\tau} - e^{\lambda t}) + \mu_3 \times (e^{\lambda t} - 1) \quad (2a)$$

$$(^{207}Pb/^{204}Pb)_{Sam} = (^{207}Pb/^{204}Pb)_1 + \mu_2' \times (e^{\lambda'\tau} - e^{\lambda' t}) + \mu'_3 \times (e^{\lambda' t} - 1) \quad (2b)$$

where Sam = sample; I = initial; μ is present-day $^{238}U/^{204}Pb$; $(\mu/\mu') = 137.88$, numerals 2 and 3 respectively stand for the second stage (duration τ or $\tau - t$) and the third stage (duration t). The first stage (not addressed here) would in general be an idealized scenario where initial Pb evolved from a primordial composition (Tatsumoto et al., 1973) in a single stage of the duration $T - \tau$, where T is estimated to be 4.55 Ga. Note that Eqn. 1a results from the division of Eqn. 1c by 1b, after minor rearrangement.

Figures 1a and 1b yield two ages of 2.55 and 2.46 Ga, for the same data. The two ages are concurrent within the calculated errors of ± 0.500 Ga. However this concurrency is of limited value in view of the large uncertainty. Thus in search for a narrowly constrained, potentially true (i.e., synchronous) age, one should not be misled by the agreement between the two diagrams, when errors are $\gg 10^6$ yr. In a modern geochemistry lab, the errors in each of the two ratios $^{207}Pb/^{204}Pb$ and $^{206}Pb/^{204}Pb$ are $< 2‰$, and would result in age-uncertainties of a few times 10^6 yr.

By definition, the data under consideration (being synthetic) have no experimental errors. Even errors arising from the decay constants are cancelled, as the isotopic make-up of each synthetic sample is concocted on the basis of the same decay constants used to establish the age-table. Thus the range in the

Table 1. Parameters of simple synthetic systems.

Date	Used in figure	Initial Pb[a] 206/204	Initial Pb[a] 207/204	τ	t	μ_2	μ_3
4-Ga isochron[b]	7	10.467	12.169	4	0	3, 5, 6, 8, 10, 12, 16	Not applicable
3-Ga isochron[b]	1, 2, 3, 4, 5, 6, 7	12.337	13.804	3	0	Same as in line above this	Not applicable
2-Ga isochron[b]	5, 6, 7	14.168	14.502	2	0	2, 4, 7, 9, 11, 13, 17	Not applicable
2-Ga disturbance[c]	1, 2, 6	12.337	13.804	3	2	(4, 5, 7.5, 11, 7, 12, 16)[d]	(16, 25, 28, 20, 4.5, 9.7, 6)[d]
0.5-Ga disturbance[c]	3, 4	12.337	13.804	3	0.5	Same as in line above this	Same as in line above this

[a] Evolved from primordial Pb (Tatsumoto et al., 1973) with $\mu_1 = 7$, for the duration $(T - \tau)$, and $T = 4.55$ Ga.
[b] Pb evolved from initial Pb in a single stage according to Eqn. 1b and 1c.
[c] Post initial lead-incorporation, Pb evolved in two stages according to Eqn. 2a and 2b.
[d] In all examples of disturbance, μ_2 and μ_3 combinations are: (4 and 16), (5 and 25), (7.5 and 28), (11 and 20), (7 and 4.5), (12 and 9.7), (16 and 6).

ages and the uncertainties exhibited in Figures 1a and 1b are due to varied configurations of the data in the two diagrams. This is also inferred from the different correlation coefficients in the two figures. Although varied, these projections are specific of the data presented; thus age-errors associated with them are termed *system-errors*, to differentiate them from experimental errors. Generally, the latter errors are too small to result in gross deviation ($\gg 10^6$ yr) from synchronism.

Variable dispersion of the data in the two diagrams is inherent in the structure of each of them. Thus while in the conventional $^{206}Pb/^{204}Pb$ vs. $^{207}Pb/^{204}Pb$ diagram (type I) the plotted pattern results from a mutual projection from the two U-Pb clocks, in a modified versions (say, type II), leads ($^{207}Pb/^{206}Pb$) from the twin clocks are referenced to one of the two. Such referencing amounts to superposition of additional modulation, relative to the conventional diagram. Thus in the example given, only perfectly closed-system-data can produce synchronous ages from the two diagrams, because they are always reproducibly projected as a line.

2.2. The Search for a Filter

A corollary to recognizing variable modulation, is recognition of its potential as a tool for objective filtration of Pb isotopic data of a disturbed system. Ideally, such filtration should result in elimination of system errors (section 2.1) and the convergence of the filtered data on a synchronous age, characterized by the same extremely narrow degree of uncertainty.

Logically, a method of filtration would have to exploit the disparity in the values of the decay constants of ^{235}U and ^{238}U, reflected in a large difference in the production rates of ^{207}Pb and ^{206}Pb. Procedurally, the requirement (in the author's mind) was to contrast the disparity in the production rates, rather than to conventionally merge their effect in a Pb-Pb diagram. With this realization, the idea of *differential Pb correlation* as a diagnostic tool and a means of filtering disturbances (or unscrambling superimposed events) became self-suggesting. This is the subject of the next section.

3. DIFFERENTIAL CORRELATIONS

3.1. Filtration by Differential Disparity

Here, as shown in Figure 2, the traditionally coupled ratios $^{206}Pb/^{204}Pb$ and $^{207}Pb/^{204}Pb$ are uncoupled, where each ratio is separately plotted against the difference between the two. The data points in each of the two figures belong to the same synthetic samples shown in Figure 1. The contrast between the patterns in Figures 2a and 2b is striking but, on hindsight, is not surprising for the reason of low production of ^{207}Pb in systems which are 3 Ga and younger. In addition, the y-axis of Figure 2b is expanded by a factor of 5, thus resulting in a degree of visual exaggeration.

In Figure 2a, line A is the best-fit line for all the data. Because the two diagrams have the same x-axis, it is possible to draw a series of vertical guideposts (dotted, marked 1, 2 and 3), in one of the figures and easily duplicate them at the corresponding identical positions in the other. In Figure 2a guidepost 1 is made to pass close to a cluster of three data points. In Figure 2b, it is seen that this cluster appears more

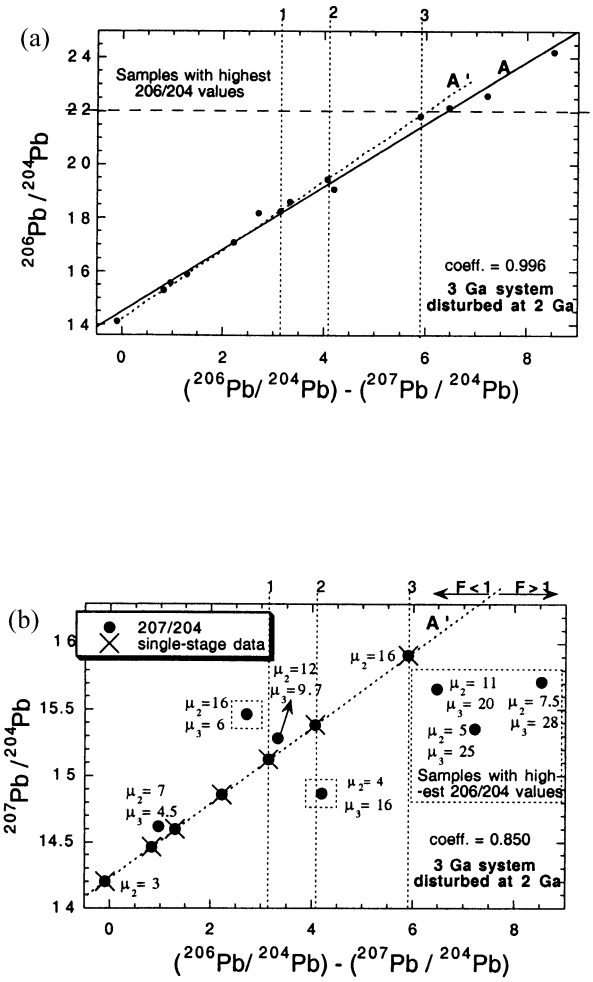

Fig. 2. (a) $^{206}Pb/^{204}Pb$ differential corrlation for a 3-Ga system which was disturbed at 2 Ga (see Table 1). Because of the almost linear production of ^{206}Pb, the data generally define a coherent line despite strong U-Pb fractionation in the disturbance. Size of the symbol corresponds to $\sim\pm 5‰$. (b) In contrast, the same data appear quite dispersed on the $^{207}Pb/^{204}Pb$ differential correlation because of the lower production rate of ^{207}Pb over the past 3 Ga, and because of expansion of the y-axis by a factor of 5. Dotted vertical lines are guideposts plotted at positions identical in both figures. Note the resolution of the clusters of data and the emergence of line A′, which is exclusively defined by all the closed-system data (indicated by a superimposed X). These evolved their radiogenic Pb in a single stage with μ_2 ranging from 3 to 16. Samples falling on line A′ are characterized by $F = 1$ (i.e., $\mu_2 = \mu_3$) while those on the left and the right of it are characterized by $F < 1$ and $F > 1$, respectively (where $F = \mu_3/\mu_2$). Thus in a glance, the disturbed samples are identified. $\mu_2 + \mu_3$ combination is shown for each of the seven disturbed samples. Size of the symbol corresponds to $\sim\pm 3‰$.

dispersed. Similarly, the two data points on guidepost 2 appear more dispersed in Figure 2b. Although expansion is a factor in the contrast, the correlation coefficients indicate that the data are actually more dispersed in Figure 2b than in Figure 2a.This fact becomes abundantly clear when the three data points to the right of guidepost 3 are considered: In Figure 2a they are almost co-linear with the datum on guidepost 3 (in an upward direction) while in Figure 2b they are distinctly scattered downwardly from it. This contrast is

consistent with U gain (relative to Pb) at a time when the production rate of ^{207}Pb was much less than that of ^{206}Pb. Quantitative estimate of U gain and loss is expressed by the fractionation factor F, defined as

$$F = (^{238}U/^{204}Pb)_3/(^{238}U/^{204}Pb)_2 \quad (3)$$

where the numerals denote second and third stage.

For the three samples under consideration, $F > 1$. They are so identified in Figure 2b and are contained within a dotted large square. From the remaining pattern a distinct linear trend emerges, particularly when two more data points falling far off the general trend are also sequestered (dotted small squares). Almost self-suggesting, line A′ is drawn in Figure 2b to pass through seven data points and miss two. It could be shown from Table 1 that the samples falling on line A′ are all the closed-system data, and those falling off it are all of the open-system type. Despite the y-axis compaction, line A′ is reproduced in Figure 2a, as the systematics would require.

Discussed next is the case of a system similar to that discussed above in every aspect except that the disturbance occurred at 0.500 instead of 2.000 Ga (data in Table 1). Because of the late date of the disturbance, the unfiltered data yield ages that are less deviant from the "crystallization" age. Specifically these ages, from type-I and type-II diagrams (not shown) are 3.10 and 3.01 Ga. The difference of 9×10^7 yr between the two ages is an indication of open system behavior. This becomes even clearer from a combined consideration of the differential correlations of such system (Figs. 3a and 3b). With the help of the guideposts, the shift of open-system data points (shown inside dotted squares in Fig. 3b) off a linear trend A′ is projected. Because of the young age of the disturbance, two samples with $F = 0.64$ and 0.81 (labeled "open" in Fig. 3b) remain too close to the closed-system line to be filtered out. This may not be viewed as a failure of the filter, because the shift of these two points is on the order of the size of the symbol of a datum (±2‰). For the same reason, line A′ could not be drawn in Figure 3a because it is barely resolved from line A (which is the best fit for all the data). The isochron-age of the partially filtered data is 3.004 Ga that is synchronous within $\pm 2 \times 10^6$ yr, and deviates from the true age by 4×10^6 yr (see Figs. 4a and 4b).

3.1.1. *Unscrambling of Multiple Isochrons*

A superimposed event can be powerful enough that it may re-homogenize the Pb isotopes of multiple samples into a *new* initial Pb, as a starting composition for further Pb evolution. Such re-homogenization need not apply to the elements (e.g., U/Pb), a circumstance that may result (with time) in the superposition of an additional linear growth. The synthetic example given here is for a two-isochron system of 3.000 and 2.000 Ga. For simplicity at this stage, the system is chosen to be free of open-system behavior. This mixture of data (see Table 1) yields non-synchronous (thus false) ages intermediate between the two actual ages, and disparate by 78 Ma (no figures). The duality of the system is readily exposed through the differential correlations, shown in Figure 5. With the help of a mere three guideposts, the best-fit line in Figure 5a is resolved into two lines in Figure 5b. These two lines correspond, of course, to the two isochrons (not shown) of the system under consideration.

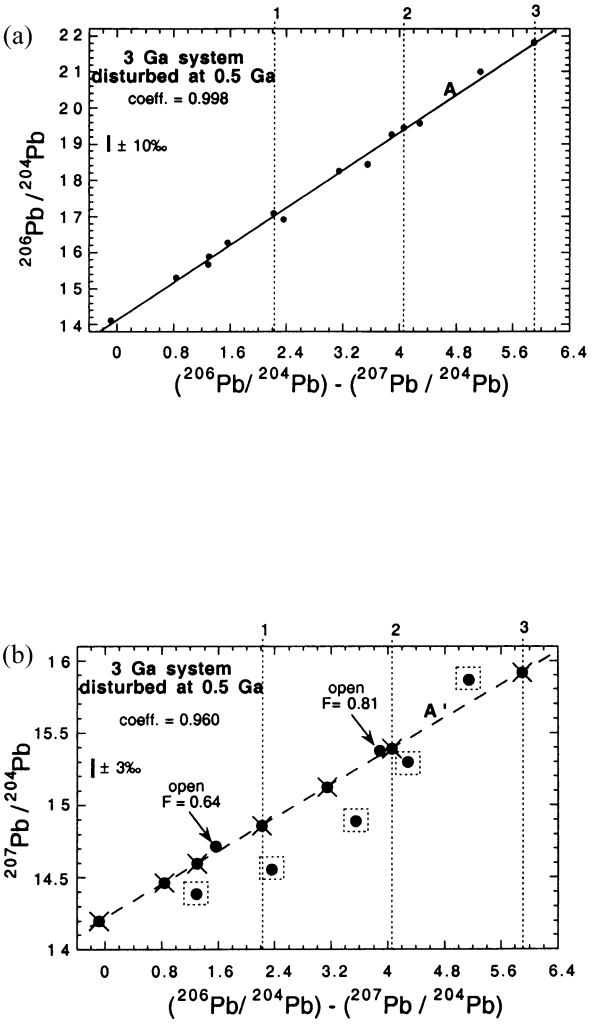

Fig. 3. (a) Differential ^{206}Pb/^{204}Pb diagram for a 3-Ga system, which was disturbed at 0.5 Ga. Line A is best fit for all the data. Guideposts 1, 2 and 3 help in tracking shifted data in Figure 3b. (b) The y-axis is expanded by a factor of 4, resulting in visual exaggeration of the shift of open-system data (some are enclosed in dotted squares) off the linear trend A′ defined by the rest of the data. Because of the "young" age of the disturbance, two samples with $F = 0.64$ and 0.81 (labeled "open") remain too close to the closed-system line, that they could not be filtered. For the same reason, line A′ could not be drawn in Figure 3a because it is barely resolvable from line A. Closed-system data are indicated by X, superimposed on the filled circles. μ_2 and μ_3 combinations are the same as shown in Figure 2b.

A more realistic variation on the theme is a dual system like the one mentioned above, with one added complication: open-system disturbance of some samples at 2.000 Ga (see Table 1). Figures 6a and 6b are the differential diagrams of the example. It is seen that the adherence of the ^{206}Pb/^{204}Pb data to a coherent linear trend is maintained. The dispersion in ^{207}Pb/^{204}Pb correlation appears complex, but the two figures concur on the linear association of the data on guideposts 1, 2 and 4. These are connected (in Fig. 6b) by a heavy solid line, which is seen to be co-linear with four data points to the left of it. The resulting linearity is indicated as a dashed line. The seven data points defining the trend yield

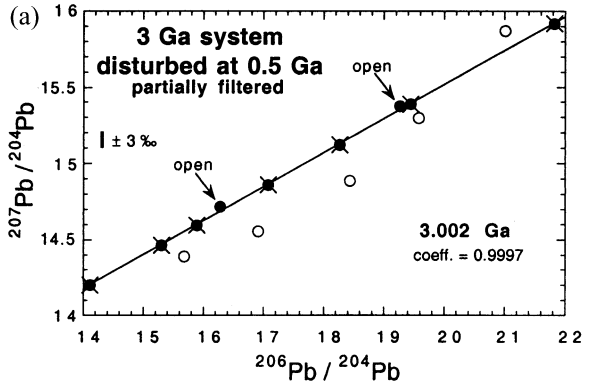

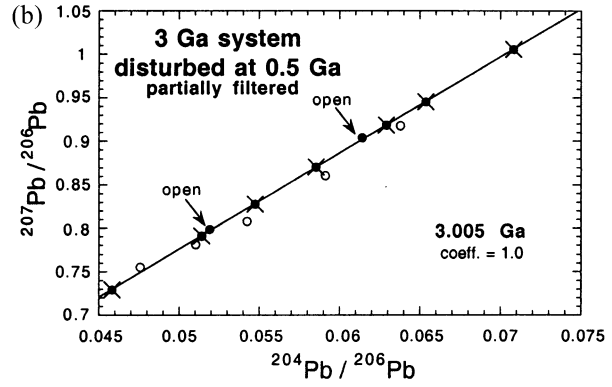

Fig. 4. (a) Isochron-age from type I diagram, for the data shown in Figure 3. Out of seven open-system data, only five could be filtered (open circles). Because complete filtration of disturbed data is not possible, the age obtained is 2×10^6 yr older than the actual age. (b) Because of varied modulation of open-systems, same partially filtered data plotted on type II diagram yield an age that is 5×10^6 yr older than the true age. Failure of the filter is associated with open-system samples where the effect of the disturbance on the isotopic budgets is negligible. Thus the resulting blemished isochrons (from Figs. 4a and 4b) are synchronous at 3.0035 ± 0.0015 Ga.

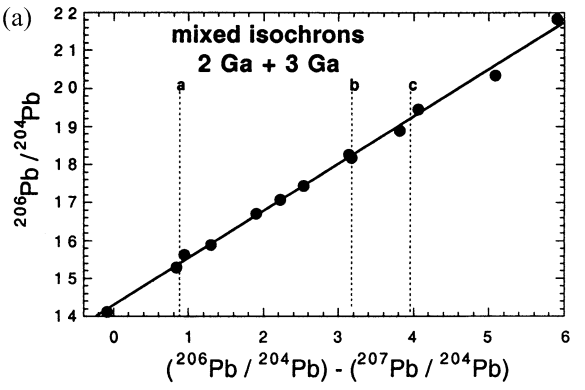

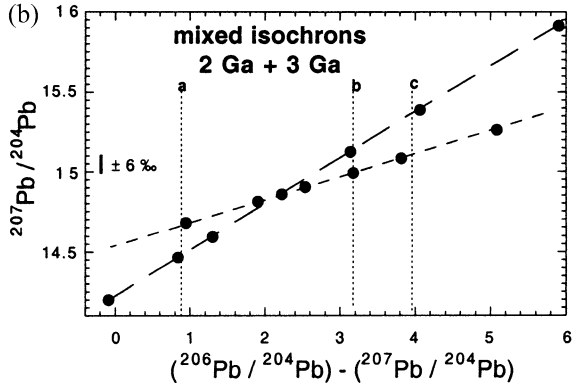

Fig. 5. (a) Differential $^{206}Pb/^{204}Pb$ correlation for a hypothetical example of a two-isochron system: one is 2 Ga and the other is 3 Ga. Despite the large difference between the two ages of the mix, the data still appear to cluster rather coherently around a best-fit line. This is largely a consequence to nearly linear production of ^{206}Pb relative to negligible build up of ^{207}Pb. (b) Differential $^{207}Pb/^{204}Pb$ correlation for the same data. With the help of the guideposts the systemic duality of the mix is revealed, as is indicated by the two dashed lines. On the age-producing diagrams, the data of each line would of course synchronously produce one of the ages, 2.000 and 3.000 Ga (not shown).

an age of 2.000 Ga, on the age-producing diagrams (not shown).

By isolating (in dotted squares) two data points dispersed at wide angles from the 2-Ga trend in Figure 6c, a second pattern of enhanced linearity emerges. This second line is defined by six points, which on age-producing diagrams (not shown) yield an age of 3.000 Ga.

In summary (see Fig. 6c), with some trial and error, two isochrons are identified and their validity is established through synchronism. Four of the six leftover samples are explicitly deviant and two appear slightly deviant (labeled "?"). In practice, some situations may be too complex to resolve completely.

3.2. Resolution by Differential Coincidence

For systems older than 3 Ga the contrast of behavior on the two differential diagrams (demonstrated in the above examples) becomes less marked and practically disappears in ~4-Ga systems. This is because in these systems the contribution of ^{235}U to the Pb budget may not be negligible. Figure 7 is an illustration of mixing three isochrons of 4.000, 3.000 and 2.000 Ga (solid, dashed and dotted lines in Fig. 7b, respectively). The non-conformity of the data to a familiar single best-fit line in the $^{206}Pb/^{204}Pb$ differential diagram is obvious. For the case on hand, the two diagrams are similar in their clear resolution of the 4-Ga isochron from the rest of the data. For the two younger isochrons, the dichotomy in resolution is clear and is a reiteration of the demonstrations in the preceding sections. Even for a more complicated system, a diagnostic feature is that an ancient isochron (perfect or not), ~4 Ga and older, will stand out as a separate trend in both differential diagrams. This condition of *differential coincidence* is characteristic of extreme an-

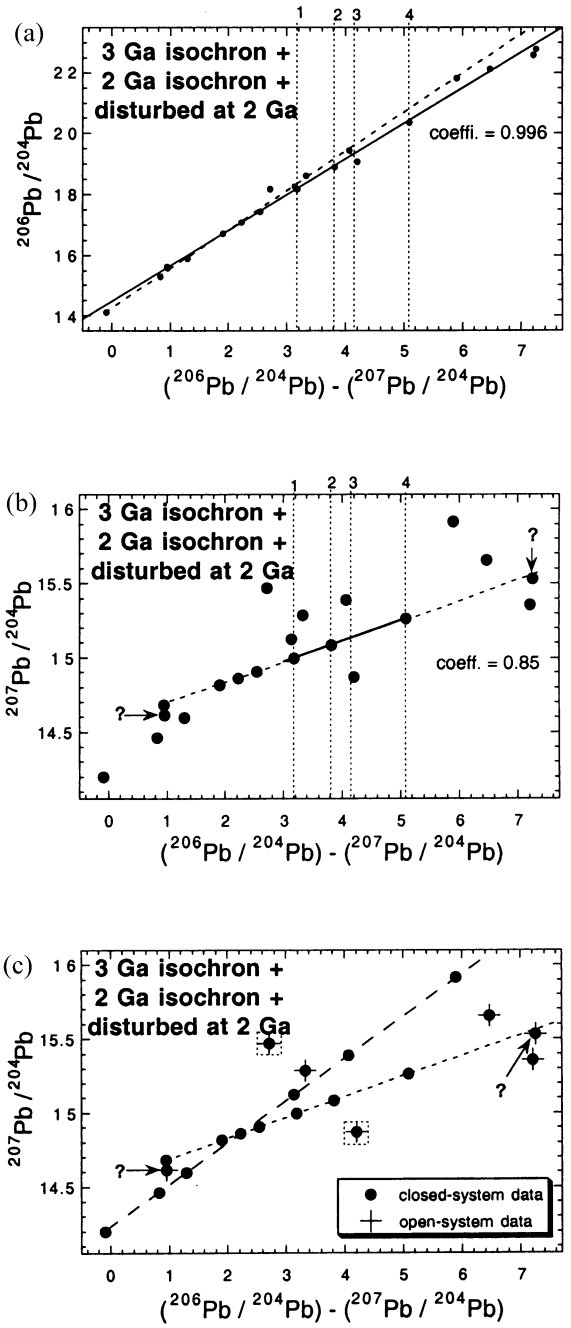

Fig. 6. (a) Differential $^{206}Pb/^{204}Pb$ correlation for a synthetic example, which is a variation on the theme of the scenario of Figure 5. Besides mixing two perfectly closed systems of 2.000 and 3.000 Ga ages, some samples became open-systems in the 2-Ga event, as prescribed in Table 1. Still, linearity is generally preserved. (b) Differential $^{207}Pb/^{204}Pb$ correlation of the same samples. The pattern appears complex but three of the guideposts (1, 2 and 4) draw attention to three co-linear data points (connected by a solid line). These, in turn, appear co-linear with four less radiogenic samples (connected by a dashed line). When extended in the opposite direction the other dashed section barely misses a datum (labeled "?"). At the other end is another sample that just misses the line. On an age-producing diagram, the seven samples forming the trend yield an age of 2.000 Ga. (c) With preliminary identification of a 2-Ga line, another general linear trend is recognized, which is enhanced by isolating (in dotted squares) two samples falling at wide angles of dispersion off the general trend. Now a second line, well defined by six more samples, becomes more

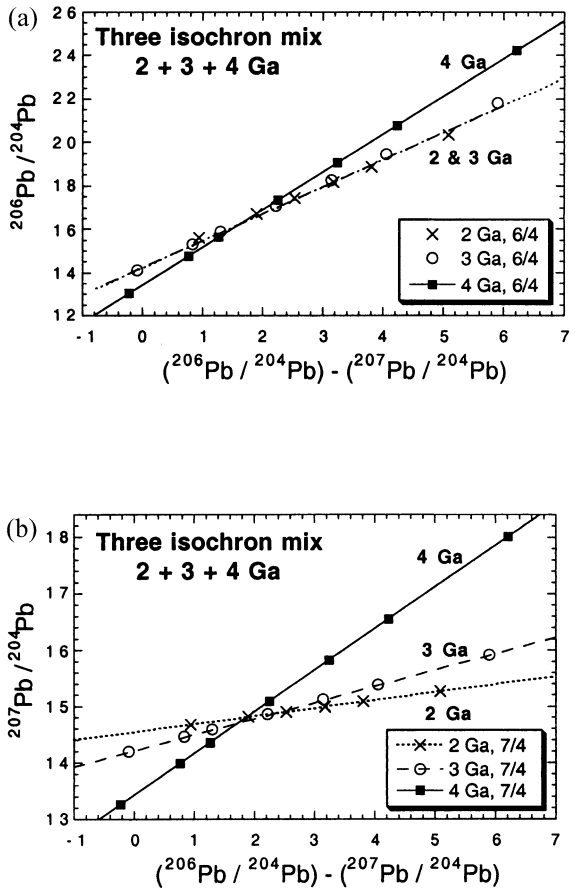

Fig. 7. (a) $^{206}Pb/^{204}Pb$ differential correlation for a synthetic mixture of three isochrons, 4, 3 and 2 Ga old. (b) $^{207}Pb/^{204}Pb$ differential correlation for the same isochrons. Note concurrence (from both diagrams) on the resolution of the 4-Ga isochron. This is termed differential coincidence, which may be useful in retrieving vestiges of isotopic imprints associated with very early planetary differentiation (see section 5.2.5). The 3-Ga and younger isochrons may be resolved on the $^{207}Pb/^{204}Pb$ correlation.

tiquity (or simulations of it, see section 4). A natural example for it is given in the application section.

3.3. Modified Differential Correlations

Among the varied reactions to the method of differential correlation is a view that the relationship as illustrated in Figure 2 is unique and unusual enough to warrant in-depth theoretical and mathematical elaboration. In truth, the specific relationship shown (Fig. 2) is one of multiple ways of expressing an aspect of the subject; that is, the shown correlation is not the crux of a concept.

If there is a crux, it is non-mathematical, namely the projection of the ratios $^{206}Pb/^{204}Pb$ and $^{207}Pb/^{204}Pb$ independent of

perceptible. Thus two isochrons are identified. Four samples are explicitly identifiable as disturbed, and two (labeled "?") are suspected of being disturbed. An open-system datum (see Table 1) is indicated by a + symbol superimposed on a filled circle.

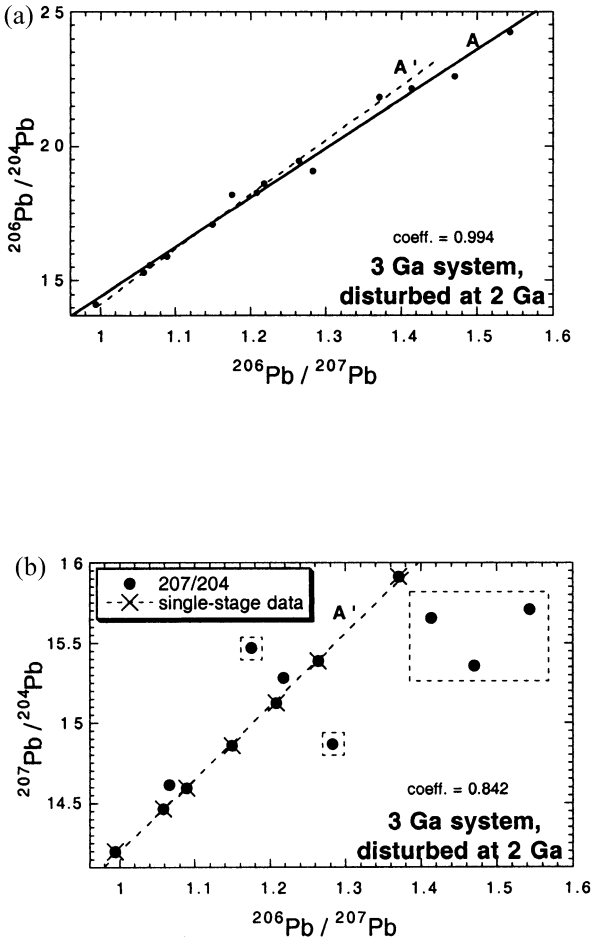

Fig. 8. (a) Same synthetic samples as in Figure 2a, plotted on a modified differential diagram. (b) Same synthetic samples as in Figure 2b, plotted on a modified differential diagram. Note preservation of the contrast between (a) and (b).

each other. Almost inherent in this concept of "differential projection" is the procedural necessity to use the same x-axis in the two projections. Here, a specific choice is largely a matter of personal preference. For example, instead of the difference between the ratios (see Fig. 2), one could use $^{206}Pb/^{207}Pb$ on the x-axis. The synthetic samples in Figure 2 are re-plotted on such modified differential correlation in Figures 8a and 8b. The figures exhibit patterns, identical in their contrast to those in Figures 2a and 2b. Again, with the help of the guideposts or any other appropriate procedure, the open-system data could be filtered out, to leave behind the closed-system line.

In terms of familiarity, Figure 8b entails a correlation between isotopic ratios, in a manner akin to the situation in an age-producing diagram. The linearity (line A′) in such correlation is the result of well-understood algebraic manipulation of the equation of radioactive decay.

As before, the amplification of dispersion beyond the effect of axis expansion in the $^{207}Pb/^{204}Pb$ correlation is attested to by the large difference between the values of the correlation coefficient in the two diagrams (Figs. 8a and 8b). That this amplification is directly related to the large decay constant of ^{235}U (that is, the non-linear production of ^{207}Pb) is easily testable by constructing hypothetical dual clocks in which the difference in the decay constants of the isotopic parents brackets the actual case. The contrast in dispersion will decrease with the convergence and increase with the divergence of the decay constants.

4. MULTI-STAGE LINEATION, A HAUNTER!

Tight agreement on a single age, from different types of Pb-Pb diagrams, is not exclusively specific to isochrons. For example, data of a perfect mixing line are perfectly synchronous. Furthermore, under a variety of peculiar fractionation-circumstances synchronous linearity may develop, which has interpretation other than being a conventional isochron. That is, and as the illustrations given next show, systemic alteration of an evolving Pb-Pb isochron, which does not destroy linearity, is theoretically possible. If it occurs, such *multi-stage lineation* can be a source of temporal misinformation. As indicated below, the conditions of such alteration are stringent. Yet, contrary to expectation, the phenomenon may be wide spread in metamorphic terrain (section 5.2). This is a weakness in the method as a geochronological tool.

4.1. Arrested Isochrons

Consider the case of an old system (say 3 Ga) whose closed-system components define an isochron at the present. Assume that at some early time (say 2 Ga ago) the system experienced a disturbance, which resulted in the complete loss of U from some of its components. In these disrupted components Pb isotopic evolution is frozen, and constitutes today a spectrum of initial leads. Because these initial leads evolved under a closed isochronous condition before the depletion of U in the disturbance, they would fall today on a line, which amounts to an *arrested isochron*, also known as paleo-isochron. In this scenario (tested numerically, but no figure is shown), the arrested isochron can pass as an ordinary isochron yielding a synchronous, yet false age, which is "older" than the system that produced it. The failure here is not of concept or of algebra but of interpretation. More specifically, it is a failure of not knowing (or ignoring) the uniform U depletion relative to the samples of the 3-Ga isochron.

The linearity of the arrested isochron derives from its two end-member constituents: (1) initial lead $(^{207}Pb/^{206}Pb)_I$ that existed 3 Ga ago when the Pb was originally homogenized, and (2) radiogenic lead $*(^{207}Pb/^{206}Pb)_I$ formed in the interval $(\tau - t)$ by radioactive decay, where τ is the crystallization age of the true isochron and t the age of the disturbance (in which U was depleted). As with a conventional isochron, the value of $*(^{207}Pb/^{206}Pb)_I$ of the arrested isochron is obtained from the slope in type-I or from the intercept in type-II diagram. In terms of calculation, the mistake would arise from the application of Eqn. 1 to the arrested isochron, instead of the proper equation for radiogenic initial Pb, given by

$$*(^{207}Pb/^{206}Pb) = (1/137.88)[(e^{\lambda'\tau} - e^{\lambda' t})/(e^{\lambda\tau} - e^{\lambda t})]. \quad (4)$$

When τ is known or assumed, the only unknown t is calculated.

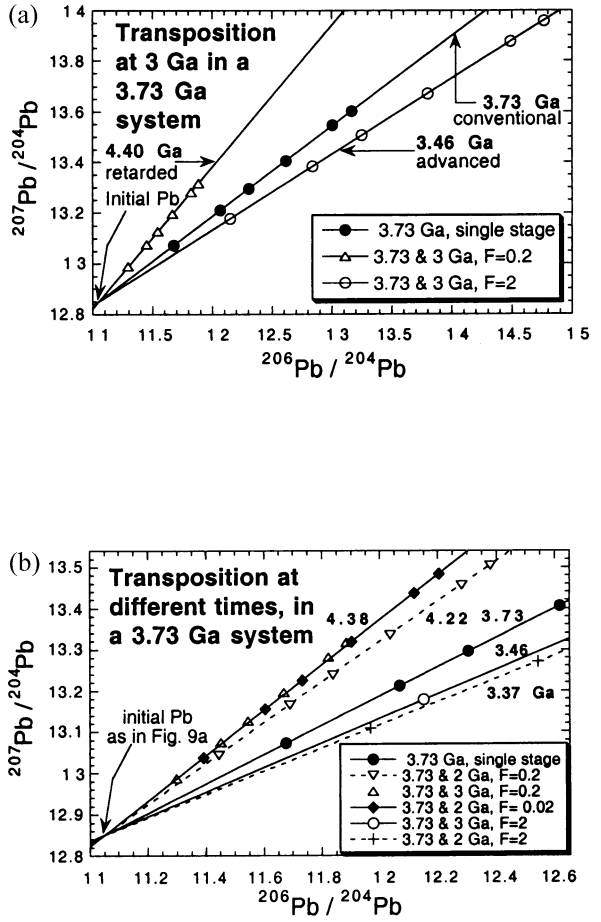

Fig. 9. (a) A uniform fractionation factor, in a disturbance, produces a line with a false single-stage age. For example $F = 2$ at 3 Ga, results in the apparent clock-wise rotation of a 3.73-Ga isochron (solid circles; same parameters as given in Fig. 10a) to yield a 3.46-Ga line (open circles). $F = 0.2$ at 3 Ga, results in a 4.40-Ga line (open triangles). Note convergence on a single true initial Pb. (b) For $F > 1$ (see case of $F = 2$), the younger the disturbance the more advanced is the "isochron." For $F < 1$ (see case of $F = 0.2$), the younger the event the less retarded is the "isochron." Also, the more retarded the "isochrons" the less readily they are resolved. All the lines shown converge on the same initial point given in (a) above.

4.2. Retarded and Accelerated (Transposed) Isochrons

From considerations of the equation of a straight line, it becomes apparent that an arrested isochron is a special case in a family of straight lines that could be constructed on the basis of Eqn. 2a and 2b. The condition for these lines is that $\mu_3/\mu_2 = F$ must have the same value for all member samples. For an arrested isochron the ratio is uniformly zero, but a value (any uniform value) different from 0 produces a line just as well. That is, the constancy of F in a disturbance results in a *linear transposition*, which mimics a true isochron. This circumstance is shown in Figure 9a where it is also seen that relative to a bonafide isochron, constant $F < 1$ causes transposition in the counter clock-wise direction (older, or retarded isochrons) and constant $F > 1$ transposes the lines clock-wise (younger or accelerated isochrons).

The above regularity-artifact is understood from Eqn. 2a and 2b, which could be reduced to

$$*(^{206}\mathrm{Pb}) = \mu_2 *(e^{\lambda\tau} - e^{\lambda t}) + f\mu_2 \times (e^{\lambda t} - 1) \qquad (2c)$$

$$*(^{207}\mathrm{Pb}) = \mu'_2 *(e^{\lambda'\tau} - e^{\lambda' t}) + f\mu'_2 \times (e^{\lambda' t} - 1) \qquad (2d)$$

where f is a constant factor. Consequently, the third stage contribution (say in %) relative to the total atomic budget remains unchanged, irrespective of the magnitude of μ_2. That is, $*(^{207}\mathrm{Pb})/^{206}\mathrm{Pb})$ of the three-stage samples is changed to a new single value, irrespective of the magnitude of μ_2. This condition, coupled with the samples' same initial Pb results in their defining a line. The commonality of initial Pb dictates the convergence of transposition-isochrons (both retarded and accelerated) on it (see Fig. 9a).

As is particularly illustrated in Figure 9b, transposition is a function of timing and fractionation magnitude. Thus a condition of severe fractionation at a later time can produce a line that nearly coincides with one produced by milder fractionation at an earlier time. This circumstance is illustrated in Figure 9b by the cases of $F = 0.02$ at 2 Ga and $F = 0.2$ at 3 Ga, with the corresponding "ages" of 4.40 and 4.38 Ga, respectively.

4.3. Translocation-Isochrons (Trans-Chrons)

This special type of three-stage lineation is characterized by the addition of the same number of Pb atoms in the third stage. That is, μ_3 is the constant in this case (see Fig. 10a). This condition (if it ever occurs) would cause rotation (relative to the true isochron) exclusively in a counter clockwise direction, on type I diagram. That is, a *translocation-isochron* (or simply *trans-chron*) invariably yields an "age" older than that of the corresponding true isochron.

One point cannot be translocated, that for which $\mu_3 = \mu_2$. This is a "dual point" common to both lines (see Fig. 10a). This is also the point around which a trans-chron appears to revolve: points to the right of the dual point "retreat" with $F < 1$, and points to the left "advance" with $F > 1$. As a result a trans-chron does not converge on initial Pb (compare with Fig. 9). A difficult requirement for this lineation is preservation of the heterogeneity imprint of the second stage, upon which is superimposed a uniformly homogeneous (in U/Pb) third stage!

4.3.1. Translocation by Terrestrial Contamination

For radiogenic meteorites (e.g., some ordinary meteorites, angrites and high-temperature inclusions in the carbonaceous meteorite Allende) translocation by terrestrial contamination may be possible. The reason is that as a component, indigenous initial Pb is often negligible, thus upon contamination with terrestrial Pb, the blank (or a homogenized composite of blank-meteoritic Pb) can become a de-facto end-member in an artifact mixing line. Troilite separated from ordinary chondrites (Unruh, 1982) often has isotopic composition that is very similar to the modern terrestrial lead (MTL) of Stacey and Kramers (1975). This strongly suggests contamination of meteoritic troilite either by scavenging of terrestrial Pb or through isotopic exchange between initial meteoritic Pb (presumably initially present in the troilite) and the environment. If the latter is the case, then initial Pb in other phases (minerals and chondrules)

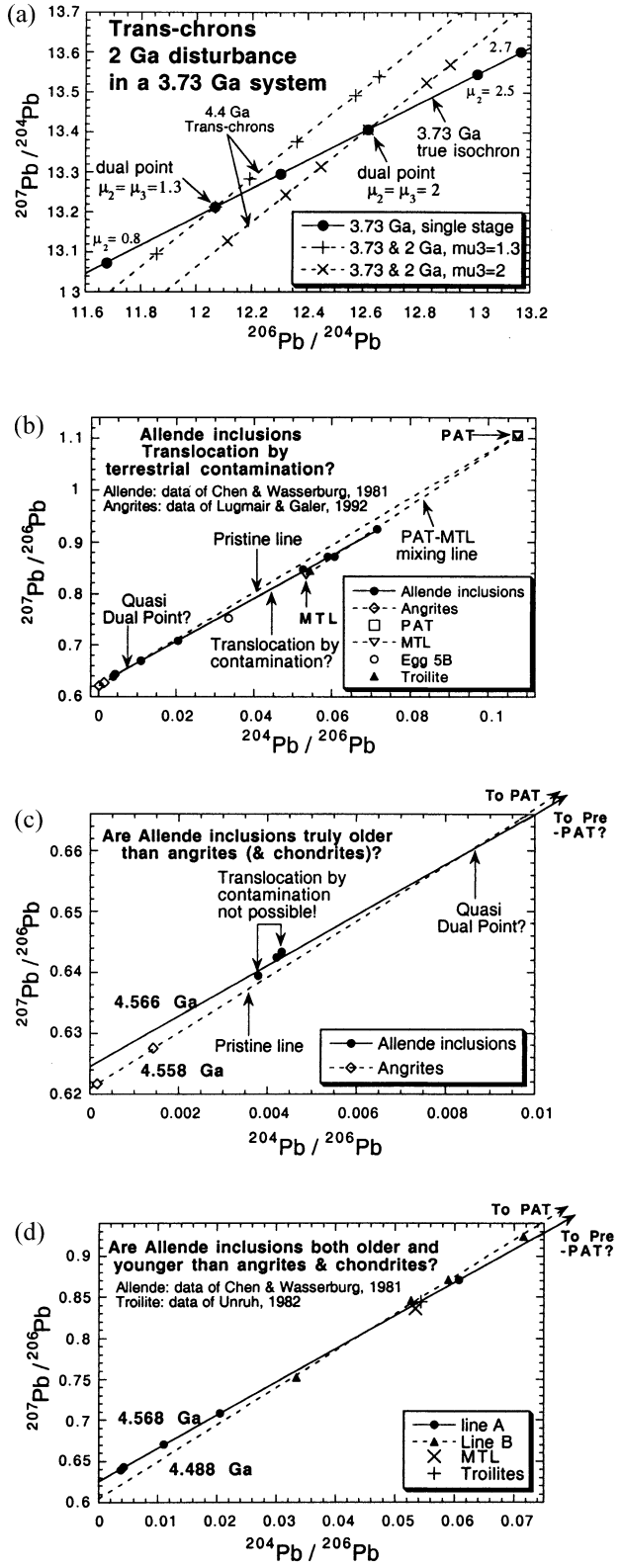

Fig. 10. (a) A uniform μ_3 produces a line with a false single-stage age. For example, 3.73-Ga samples which experienced a change to a single value for μ_3 at 2 Ga will define a line (a trans-chron) with an apparent single-stage age of 4.4 Ga. The point of intersection with the true isochron (of the undisturbed samples, filled circles) is a dual point characterized by $\mu_2 = \mu_3$. Trans-chrons of the same disturbance have the same "age," that is, they are parallel lines. Trans-chrons are always "older" than the true isochron. Also, the older the disturbance the older is the trans-chron. As with all synthetic isochrons in this work (see Table 1) $\mu_1 = 7$; μ_2 values are shown. (b) Contamination of radiogenic samples (e.g., Allende inclusions) with modern terrestrial lead (MTL) may result in a linear translocation. The line of Allende inclusions passes through MTL, suggesting contamination. Also, its extension (not drawn) passes to the right of PAT, which is forbidden by the systematics, unless the inclusions predate accretion of planetary bodies and thus contain primordial Pb that is more primitive than PAT. In this case passing through MTL is accidental. (c) Two angrite samples fall on a line consistent with PAT, that intersects the line of Allende inclusions at a Quasi Dual Point (QDP) around which the Allende line might have rotated to an older age. However, in this case the three samples to the left of QDP (filled circles) should have lagged behind. (d) Adding further to the ambiguity is the fact that the Allende inclusions' points may fall on two lines, one is consistent with PAT, and the other passes to the right of it, suggesting a more primitive "Pre-PAT" initial. That is, Allende inclusions may be both older (4.568 Ga) and younger (4.488 Ga) than the angrites and the chondrites (see section 5.5 and Fig. 29).

may be also susceptible to contamination through exchange; that is, being radiogenic is not a guarantee for being free of contamination.

In Figure 10b it is seen that the less radiogenic Allende inclusions (data of Chen and Wasserburg, 1981) fall on a PAT-MTL mixing line. (PAT, the nick-name of the late Claire Patterson, has long been used to denote *Primordial Pb*, which he discovered [Patterson, 1956], and which was confirmed and refined by Tatsumoto et al. [1973]). Within error, however, these data points define with the more radiogenic samples an excellent line (coefficient of correlation = 0.9998), corresponding to an age of 4.566 Ga.

In contrast to Allende inclusions, with a trajectory far to the right of PAT, two angrite samples (from the work of Lugmair and Galer, 1992) are co-linear with PAT at the younger age of 4.558 Ga (Fig. 10c). The two lines intersect at a *Quasi Dual Point* around which the inclusions' line might have rotated as a result of contamination with MTL. If so then the 4.566-Ga age is invalid. This matter is addressed in section 5.5.2. Suffice it here to point out the similarity (in effect) to translocation through geochemical fractionation in a disturbance (compare Fig. 10a with Figs. 10b and 10c). Figure 10d is discussed in section 5.5.2.

4.4. Chronoplane

This term is applied to a spatio-temporal plane, which may unfold as a result of the superposition of a translocation-disturbance (see section 4.3) on a contained system, in which the imprints of both events (crystallization and disturbance) co-exist. I included this peculiar dual mode after realizing it appears to apply to the magma of Hawaii.

Consider the case of a contained source, S (a magma chamber or a mantle cell), say 4.55 Ga old, which was differentiated, once strongly at 3.25 Ga, and once mildly at 0.9 Ga. The two dates are chosen on the basis of observations discussed in the application part (sections 5.6.2 and 5.6.4). The scope of the 3.25-Ga event is the entire system which if thoroughly sampled (as the example assumes), its present day Pb-Pb data would extend symmetrically on either side of the parental source (filled circles, Fig. 11a).

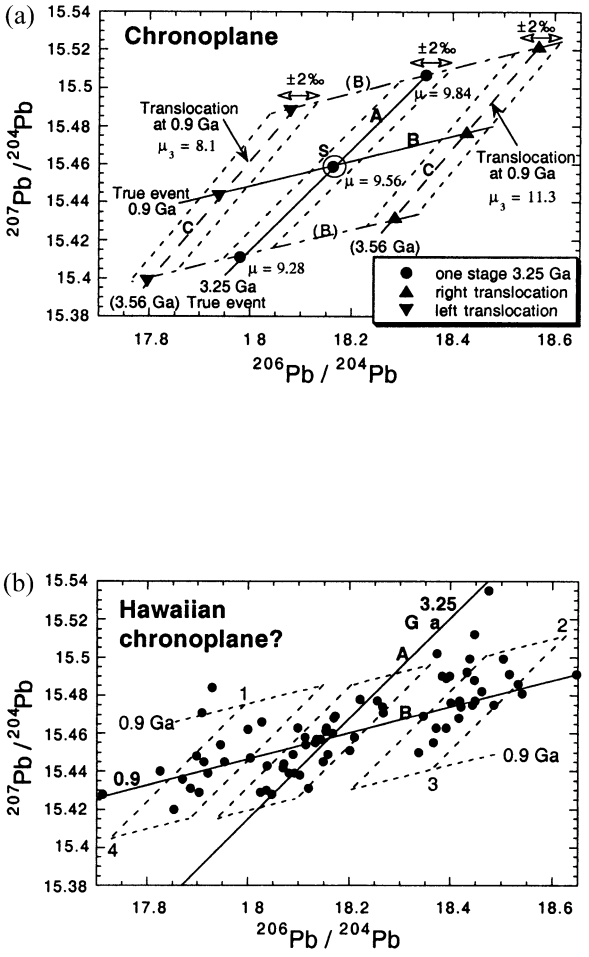

Fig. 11. (a) An idealized, two-event chronoplane. S is an ancient parental source, which was partially fractionated, once at 3.25 Ga (solid line A, filled circles; $\mu_1 = 7$; μ_2 ranges from 9.28 to 9.84) and a second time at 0.9 Ga (solid line B). These two lines (with far more data points than depicted) may be identified through filtration by the differential correlation procedure. The second event is characterized by bipolar fractionation, possibly through U enrichment in a mobile accessory phase that itself is enriched in one domain ($\mu_3 = 11.3$), leaving the other depleted ($\mu_3 = 8.1$). Being mild, the second event does not erase Pb isotopic heterogeneity in the major rock-forming minerals. This, combined with the bipolarity of μ_3, results in the unfolding of a chronoplane, the longitudinal borders of which are two mirror-image translocation isochrons (large dashed lines C). Each line is broadened (±2‰) to allow for additionally superimposed minor complications. The latitudinal borders of the field (dashed-dotted lines) run parallel to line B, and their separation is a measure of the degree of fractionation in the A-event (assuming thorough sampling). (b) The Hawaiian Pb data are seen (or possibly imagined) to fall into three resolvable clusters, each of which is possibly a "demi parallelogram." These are contained within an encompassing parallelogram 1, 2, 3, 4. In theory (see text), the two flank-clusters were derived at 0.9 Ga from the central cluster, which is the product of a 3.25-Ga event.

For the purpose of factualism in the model, the Hawaiian Pb-Pb data (original authors cited in Zindler and Hart, 1986) are shown in Figure 11b, together with the model's two imprinting isochrons (3.25 and 0.9 Ga), plotted to intersect each other in the center of the field. The premise of the model is that the scatter of the data in Figure 11b is controlled by a mechanism that approximately replicates the pattern of the ancient event (3.25-Ga trend) along the trajectory of the superimposed event (0.9-Ga trend). As a result a chronoplane in the shape of a parallelogram unfolds (outlined by points 1, 2, 3, 4 in Fig. 11b). With some imagination the data appear to fall in three clusters, each constituting a demi-parallelogram within an encompassing one. If so, the apparent replication observed in the Mauna Kea lava on the micro-scale (section 5.6.4) may be extended to the macro scale of an entire hot spot!

The scenario is expressed quantitatively in Figure 11a by a central isochron, flanked by two translocation-isochrons (filled triangles). Translocation-lineation (section 4.3) requires that the flank-isochrons appear "older" than the central one; specifically their slope corresponds to a false 3.56 Ga age. The existence of two translocation-isochrons requires that U-Pb fractionation in the disturbance event be *bipolar*. That is, the extent of U-enrichment (to a single μ_3 value) in some samples (linearly shifted to the right in Fig. 11b) is at the expense of depletion in others (shifted to the left).

The survival of the two imprints (3.25 and 0.9 Ga) need not be contradictory and may be affected through the mild nature of the second event, which mobilizes, say, a susceptible (U-rich) accessory phase without affecting serious re-equilibration in the major minerals. Thus the isotopic heterogeneity of samples fractionated in the crystallization stage is largely preserved. Being of uniform chemical composition, the mobilized phase may have a single μ, and if it is U rich, it may impart its imprint to the host. As to the bipolarity of μ_3 (see Fig. 11a), it may be achieved through uniform enrichment of the accessory phase into one domain (effective $\mu_3 = 11.3$), at the expense of its depletion from another (effective $\mu_3 = 8.1$).

As a consequence to bipolarity (mentioned above), the resulting translocation-isochrons (large dashes) would become the longitudinal borders of a chronoplane (Fig. 11a). The highest and lowest μ_2 values of isochron "A" would fall on the latitudinal borders of the plane. These are lines (dashed-dotted, possibly imaginary), which bracket and run parallel to isochron "B." The net result is a symmetrical *chronoplane* with the source being located at its center. In Figure 11a, the 3.25-Ga isochron and its translocation images are plotted each within a band corresponding to ±2‰ error on the x-axis. This is to allow coverage of system errors (section 2.1) in an actual system. Interestingly, when superimposed on the isotopic field of Hawaiian lava, 84% of the data fall inside the plane, and the majority of the points fall within the three envelopes of Figure 11a (detail in section 5.6.4).

5. APPLICATIONS

5.1. Answering Questions With Questions?

In dealing with isotopic data one is often (in fact to a degree, always) dealing with an interpretive component, a circumstance that may result in controversy. An aspect of a controversy may stem from imperfect data that permit varied subjective perceptions. In general, one expects good data-filtration to weed out subjectivity and thus lessen controversy. This has been an objective of the proposed methodology. Yet its application to the Amîtsoq gneisses appears to have increased the controversy surrounding their true age. Instead of deciding "the age," three

distinct ages are indicated. Furthermore, two of these ages differ widely from anything published earlier on the topic. One of the ages is so old (4.42 Ga) that, if taken literally, suggests the potential survival of a piece of a very ancient terrestrial crust, faintly recalling a lunar scenario. Alternatively, in a reconciliation scenario these ages are considered artifacts. That is, the exotic mechanisms of "multi-stage lineation" discussed in section 4 may not be at all exotic. In either case, instead of narrowing the controversy surrounding "the age" of the Amîtsoq gneisses, it could be argued that the author expanded it.

Similarly, applying the filtering procedure and the synchronism concept to OIB appeared for a short while to decide the issue of ocean-island magma generation, in favor of one model, that of Chase (1981), who argued that the Pb-Pb linear arrays of OIB are more reasonably interpreted as secondary isochrons than as mixing lines. That the corroboration may not be that simple became apparent from examination of the high-precision Pb data on Mauna Kea (Abouchami et al., 2000) which appear to define a highly organized pattern of dispersion. Over 85% of the data fall on four distinctly resolved parallel lines. Three of the lines yield the same "age" of 3.23 ± 0.03 Ga! With this in mind, re-examination of the large body of data on Hawaii (original authors are in Zindler and Hart, 1986) revealed apparent existence of the linear parallelism, but on a coarse scale (see Fig. 11b). In its coarseness each of the linear "ribbons" could be seen as a miniaturization of the shape of an encompassing field, a parallelogram. Tentatively, the encompassing parallelogram is interpreted as a spatio-temporal plane, representing a geometric unfolding, caused by the superposition of two families of isotopic trajectories (each being the expression of an isochron, or a simulation of it), thus the term chronoplane (see section 4.4). Here again, the search for an answer seems to have opened the door for new questions.

Other examples of enlarging the "interpretive component" are to be found in the "observation" of a low-μ crustal reservoir (section 5.3), and in the inference to the existence of ancient ($\sim$4.4 Ga) profiles in some of the zircons data (section 5.4).

It is possible that the applications presented raise more questions than they provide answers. It is also possible that intensification of ambiguity is transiently inherent in finer resolution, and with replication of phenomena and increased capacity to sort out, advancement will be the eventual outcome.

5.2. Filtered Isochrons of Crustal Rocks—Ages and Errors

In this section some of the filtered isochrons, used in the tentative identification of a U-poor crustal reservoir (see section 5.3), are presented. The Vikan gneiss of North Norway (Taylor, 1975) acquires special importance in the present presentation, as its inferred isochrons participate in multiple intersections. This ubiquity could be accidental, an ambiguity that extends to the very concept of inferring a reservoir on the basis of a given group of isochrons. What is shown is merely a group of synchronous lines, which are found to intersect at a point. That the point of intersection gives the present-day composition of a common parental source is a matter of faith that such regulated condition is not an accident.

As to the synchronous isochrons shown, it should be pointed out that for synchronism to be an objective criterion for filtration, it has to be the singular defining factor; thus no consequential a priori assumptions have been made regarding the quality of the data under consideration. Concerning errors, synchronism is subject to the general experimental condition that precision is often not a measure of accuracy. Thus errors in synchronism may not be directly applicable to the calculated age. The case of the synthetic data in Figure 4 may serve to illustrate the point. Here the age-line contains two unresolved open-system data points, resulting in a synchronous age of 3.0035 Ga that is imprecise by $\pm 1.5 \times 10^6$ yr. This range of uncertainty, however, does not cover the actual age of 3.000 Ga.

In this report age calculation and error estimates were obtained from Isoplot/Ex (Ludwig, 2001), using the uncertainties which have long been adopted in this laboratory. These are $\pm 0.11\%$ and $\pm 0.17\%$ for $^{206}Pb/^{204}Pb$ and $^{207}Pb/^{204}Pb$, respectively. In all cases the calculated "Isoplot-age" of a given data set agrees with the "synchronism-age" to within a few 10^6 yr, but the errors in the former are typically over an order of magnitude larger than in the latter. Being applied to filtered data in which the filter removes "system errors," the age errors from the Isoplot method may be exaggerated (by a factor of 5?). However, unless it is shown that a developed state of synchronism is free of artificial lineation, or a method is developed to guard against it (when present), the tight reproducibility of a synchronism-age remains a mere procedural criterion for the quality of filtration.

Occasionally, synchronism allows the apparent unscrambling of superimposed events in a disturbed geologic terrain. Three examples of unscrambling are presented in this report: the Vikan gneiss of Norway (data of Taylor, 1975), the Lewisian gneiss of Scotland (data of Chapman and Moorbath, 1977) and the Amîtsoq gneiss of Greenland (data in Kamber and Moorbath, 1998). In all three cases each of the resolved isochrons is reproduced (in multiple Pb-Pb diagrams) to within a few million years. Yet, since independent validation of the reported multiple events is not immediately possible, the reported ages may be taken with reservation.

5.2.1. The Vikan Gneiss, North Norway

The differential diagrams of this gneiss are shown in Figures 12a and 12b, on the basis of which five data points (shown in boxes) are filtered out. The filtered data are found to yield a synchronous age of 3.401 Ga (not shown). Apparently this single age is not unique, because closer examination of the $^{207}Pb/^{204}Pb$ differential correlation shows it to be compatible with resolution into two lines (Fig. 13a). Furthermore, the two lines appear to be reproduced in an expanded $^{206}Pb/^{204}Pb$ differential correlation (Fig. 13b). The resolution implies a case of differential coincidence (see section 3.2), tenuous as it may be, because of the closeness of the ages and the convergence of the daughters' production rates at this region of the age spectrum. With minor change and additional correlated filtration, the two ages of the Vikan gneiss are 3.761 and 3.391 Ga, which are synchronous within 2×10^6 and 10^6 yr, respectively (Fig. 14a and 14b). The closeness of the age from the single-age scenario to the younger age in the two-age scenario, appears to suggest emplacement at 3.76 Ga and a superposition of an event at 3.39 Ga. This is the view adopted here. However, if the

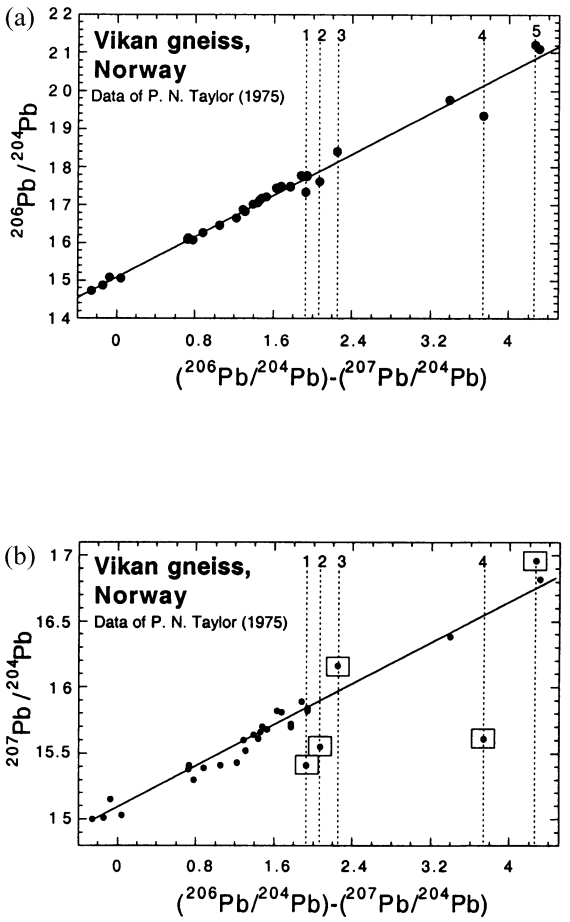

Fig. 12. (a) $^{206}Pb/^{204}Pb$ differential correlation for the Vikan gneiss, with five guidepost passing through samples falling off the best-fit line. (b) $^{207}Pb/^{204}Pb$ differential correlation for the same samples. Line through data is hand drawn to mimic the line in (a). Deviation of the five data points (in boxes) is clearer. When these are filtered out, the remaining data yield a synchronous age of 3.401 Ga (not presented).

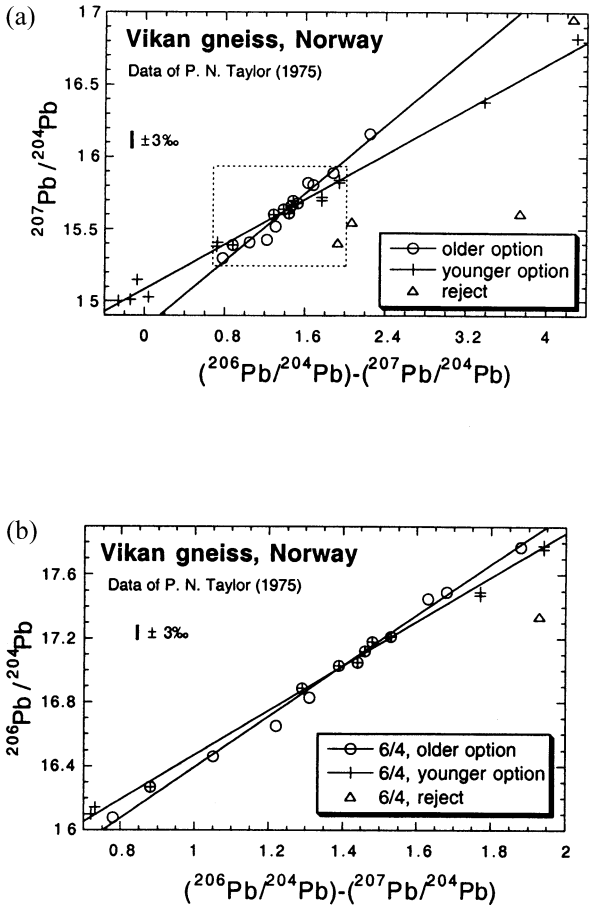

Fig. 13. (a) Careful examination shows that the Vikan gneiss data may be resolvable into two trends in the $^{207}Pb/^{204}Pb$ differential diagram. A rejected point in Figure 12b is part of the older trend here. (b) Data within the dotted box in (a) are plotted on an expanded scale where the $^{206}Pb/^{204}Pb$ data appear to tenuously corroborate the resolution into two lines.

steeper slope was produced by a translocation-disturbance (section 4.3), the older age would not be valid. Knowledge of the μ values of the samples could elucidate the issue.

5.2.2. *The Vredefort Dome, South Africa*

Excluding the data on the Outer Granite Gneiss (OGG) because of its younger age, the remainder of the data on the Vredefort dome (Hart et al., 1981) are shown in Figure 15. These are referred to by the original authors as ILG (Inlandsee Leucogranofels) and SMZ (Steynskraal Metamorphic Zone). It is seen that filtering out 28% of the data results in an age of 3.270 Ga that is synchronous to within $< 10^6$ yr. The simple pattern of the data does not require the use of differential diagrams.

5.2.3. *The Lewisian Gneiss, North-West Scotland*

The simple linearity of the data on this gneiss (data of Chapman and Moorbath, 1977) requires no mediation by the differential procedure for filtration. Dual Pb-Pb presentation, however (Figs. 16a and 16b), appears to suggest two superimposed events of 2.688 and 2.271 Ga. In theory, the older age could be in error if its line is a translocation-isochron. Taken at faith value, these ages are synchronous (on all Pb diagrams), each to within 10^6 yr or less. In contrast, the unfiltered data yield ages on types I and II diagrams that differ from each other by 2×10^7. The calculated age of the unfiltered data is 2.700 $\pm$ 0.092 Ga.

5.2.4. *Broken Hill, Australia*

Here, filtering out two data points out of 11 (data of Reynolds, 1971) results in a highly reproducible line which, from all three types of Pb-Pb diagrams, yields an age of 1.874 $\pm$ 0.0004 Ga. Figure 17 is a partial illustration. The unfiltered data yield an age of 1.659 $\pm$0.073 Ga. Including the two reject data points results in a shallower slope, thus the younger age.

5.2.5. *The Amîtsoq Gneisses, West Greenland*

When whole-rock Pb isotopic data on the Amîtsoq gneisses (further expanded and summarized by Kamber and Moorbath,

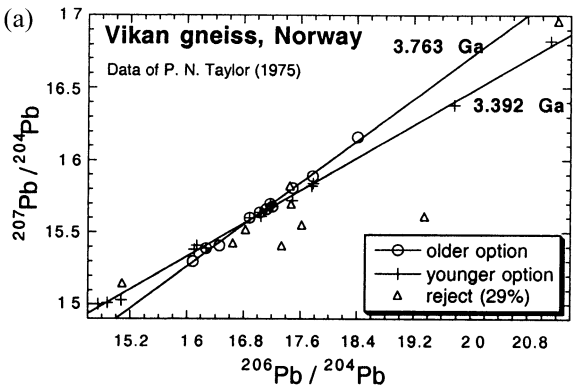

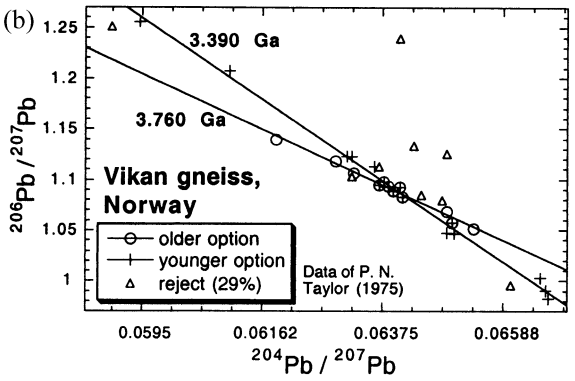

Fig. 14. (a) On a type I Pb-Pb diagram the Vikan gneiss data appear compatible with two isochrons. (b) The two isochrons are synchronously reproduced on a type III diagram. Calculated by the isoplot program (see section 5.2.) the ages are 3.76 ± 0.08 and 3.39 ± 0.04 Ga.

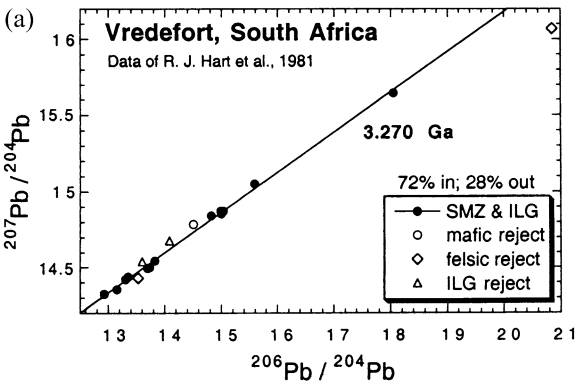

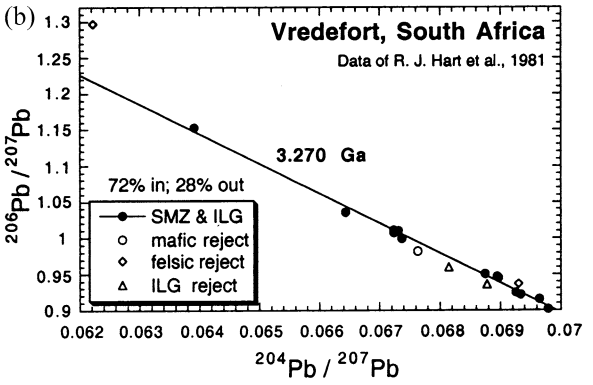

Fig. 15. (a) Data on the Vredefort dome (excluding granites) are shown on a type I diagram. (b) Same data plotted on a type III diagram. The lines of the two diagrams are highly synchronous when 28% of the data are filtered out. Standard age calculation for the filtered data (section 5.2.), yields exactly the same age but with ±0.051 Ga.

1998) are plotted on types I and II diagrams, they yield an age of 3.54 Ga (no figure shown) that is non-synchronous by $\pm 1.5 \times 10^7$ yr. Elimination of a few samples does not correct the disparity in the results. This is not surprising, as these are rocks of different lithologies and are generally seriously metamorphosed and deformed.

Of particular significance is the visible dispersion of the data on the $^{206}Pb/^{204}Pb$ differential diagram (Fig. 18a), suggesting the existence of an ancient imprint far older than the approximate age of 3.54 Ga. Furthermore, 30% of the data (11 out of 37) fall on a well-defined linear trend (labeled A) at a distinct angle relative to the rest. Line A appears reproduced in the $^{207}Pb/^{204}Pb$ differential diagram (Fig. 18b), suggesting a condition of *differential coincidence*, where the line is potentially associated with an ancient discrete event (see section 3.2). Indeed, when the data of line A are plotted on the age producing diagrams (Figs. 19a and 19b) they yield an age of 4.419 Ga, which is synchronous within $\pm 1.5 \times 10^6$ yr. However, like any other perfect line, the temporality of line A may be subject to interpretations other than being a straightforward isochron.

The $^{206}Pb/^{204}Pb$ differential correlation for the remaining 70% of the data is shown in Figure 20a, where the points cluster around a best-fit line (coefficient = 0.996). In contrast, the data are more scattered in the $^{207}Pb/^{204}Pb$ diagram (coefficient = 0.962, best-fit line not shown). With the help of duplicate guideposts (labeled 1 through 8) in the two diagrams, a regularity in the pattern of dispersion in Figure 20b seems to emerge. For example, at guideposts 2, 3 and 6, the data appear to be resolved into two linear trends. The delineation of the lower line is further indicated by the shift of the two data points of lines 7 and 8 toward it. There is a suggestion in both diagrams that the point on line 5 is aberrant. Three additional points are also suspected (open symbol).

Guided by the above indications from Figure 20, the data are tentatively divided into two additional groups: B and C (the third group [labeled A] is shown in Fig. 18). These when plotted on the age-producing diagrams indicate two ages of 3.454 and 3.738 Ga (Fig. 21), which are synchronous within $\pm 5 \times 10^5$ and $\pm 2 \times 10^6$ yr, respectively. The following is a summary of the scenario under consideration:

Line A (11 points) = 4.419 ± 0.0015 Ga
Line B (13 points) = 3.738 ± 0.002 Ga

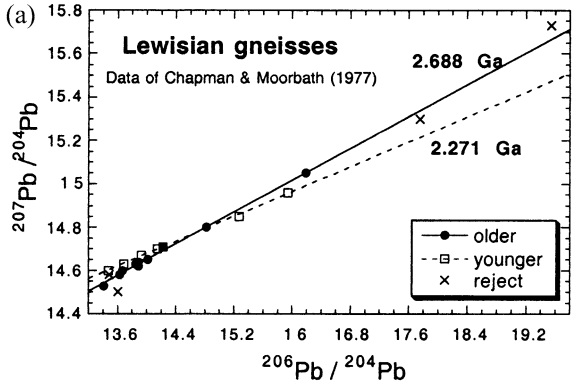

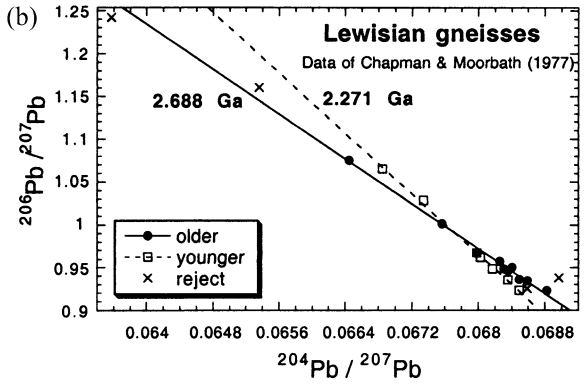

Fig. 16. (a) The Lewisian gneisses appear to indicate two events occurring at 2.688 and 2.271 Ga. The age of the unfiltered data is 2.683 Ga, which is non-synchronous by ±0.015 Ga. (b) The presumed isochrons in type I diagram are reproduced on type III within $< 10^6$ yr. Within a few million years, the same ages are calculated by the standard procedure, but with ±0.08 and ±0.12 Ga uncertainty in the older and younger age, respectively.

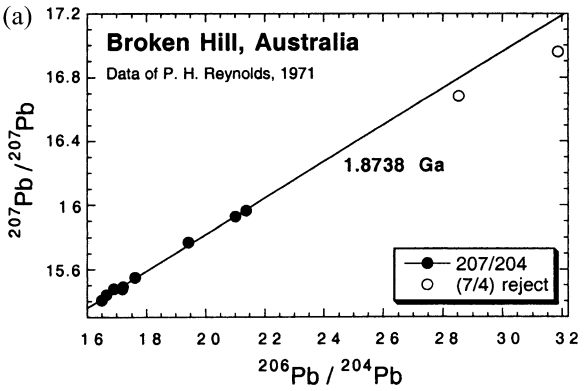

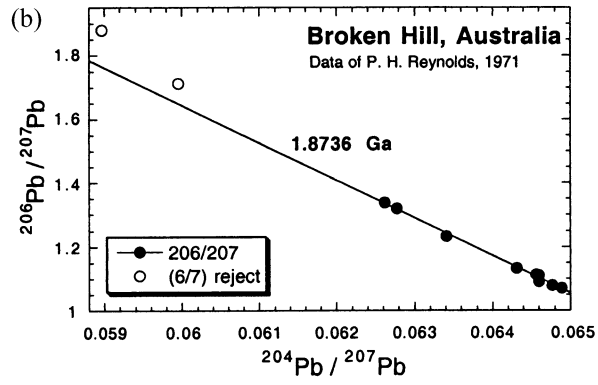

Fig. 17. (a) Data of Broken Hill rocks on a type I diagram. Inclusion of the two rejected samples results in a younger age of 1.661 Ga, which is marginally synchronous by $\pm 5 \times 10^6$ yr. (b) Filtration of two data points out of 11 results in a line of 1.874 Ga that is synchronous by all three types of diagrams, within $\pm 4 \times 10^5$ yr. Calculation by the standard procedure results in the same age but with ±0.07 Ga.

Line C (9 points) = 3.4545 ± 0.0005 Ga
Reject (4 points)

Multi-stage lineation was thought to be rarely operative, because of the stringent requirement of a uniform constancy in the third stage (see section 4). This, in addition to over estimating the significance of synchronism, led the author to consider the above mentioned ages as valid (Tera, 2000a and 2000b). In this report an explanation of lines A and C as being the result of multi-stage lineation, is brought to the fore. In addition, at least as an intriguing exercise, another scenario is presented in which the validity of the 4.4-Ga age (of line A) is assumed. In both scenarios, line B is accepted as a true isochron. Its age of 3.74 Ga falls within the range of ages (3.65–3.85 Ga) considered for the Amîtsoq gneisses.

5.2.5.1. A reconciliation scenario. Two of the three dates mentioned above differ widely from the ages of these gneisses, published over a period of three decades. Consequently one is compelled to consider that lines A and C (Figs. 19 and 21) are not true isochrons. A reconciliation scenario outlined here explores the possibility of deriving the artifact lines from line B (the only true isochron), via one or more of the mechanisms of lineation discussed in section 4. The older "age" of line A would require counter clock-wise rotation of the linear correlation, on a type I diagram.

The numerical exercises in section 4.3 showed that a 3.73-Ga system, disturbed by translocation at 2 Ga can produce a line with the artifact-age of 4.4 Ga (see Fig. 10a). Assuming the applicability of the mechanism, this fact specifies the same disturbance time (2 Ga) for the Amîtsoq. This is because a specific artifact-age due to translocation is dependent solely on two parameters: the age of the system (given by the parent isochron) and the time of the disturbance. Note that line A could not be derived from line B by transposition (i.e., disturbance via constant fractionation factor *F*), because this mechanism requires conversion of the two lines on a single end point (see section 4.2), which is not the case here (no figure).

In contrast to translocation, an artifact-age produced by

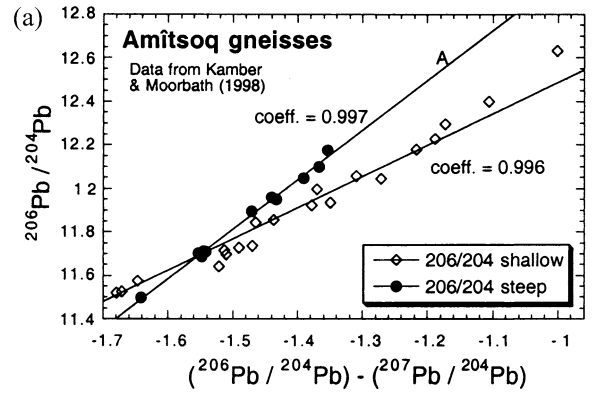

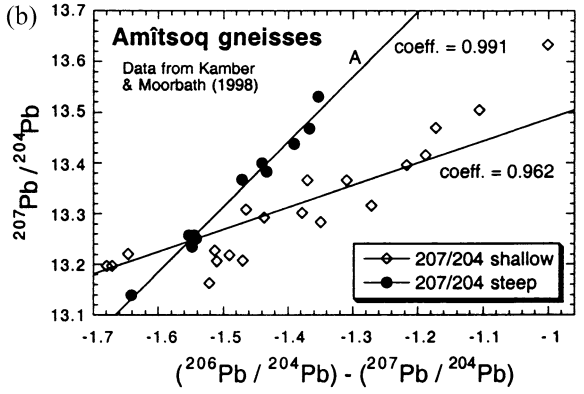

Fig. 18. (a) Differential $^{206}Pb/^{204}Pb$ correlation for the Amîtsoq gneisses. Note obvious bimodality: 30% of the data falling rather precisely on line A; the rest of the data clustering around another line, which is defined by additional six data points falling outside the range shown. (b) Note coherent reproducibility of line A, suggesting a condition of differential coincidence (see text).

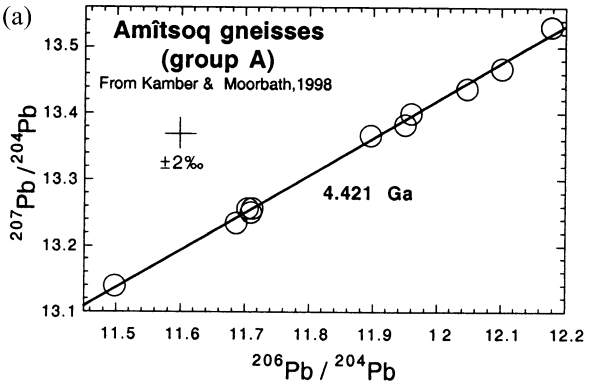

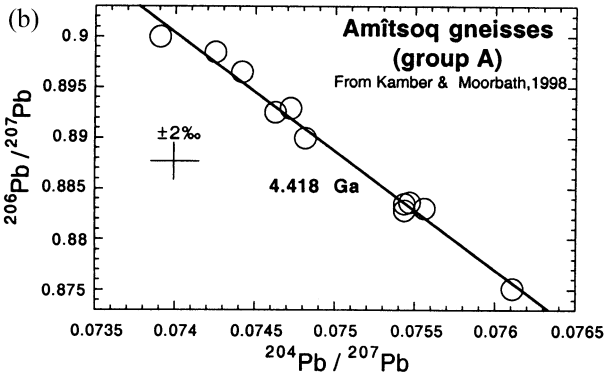

Fig. 19. (a) Data of line A in Figure 18 plotted on type I diagram. (b) Same data plotted on type III diagram. Standard age calculation results in 4.416 ± 0.06 Ga.

transposition is dependent additionally on the magnitude of F. For the Amîtsoq's line C, the younger artifact-age suggests $F > 1$ (see section 4.2). If one assumes the same time for the disturbance (2 Ga), then $F = 1.7$. A characteristic of transposition is that irrespective of the magnitude of F or the time of the disturbance, a transposition-line of a given system always intersects the parent isochron at the same point, which corresponds to initial Pb (see Fig. 9). In fact, even in absence of a true isochron, two transposition lines would intersect at a point corresponding to initial Pb of the missing (i.e., obliterated by transposition) isochron (see Fig. 9).

For the case on hand, lines B and C intersect at $^{206}Pb/^{204}Pb = 11.065$ and $^{207}Pb/^{204}Pb = 13.023$. Subtracting primordial Pb (Tatsumoto et al., 1973), one obtains for the first stage (the interval 4.56–3.73 Ga) $\mu_1 = 7.17$, based on $^{206}Pb/^{204}Pb$. From $^{207}Pb/^{204}Pb$ one obtains $\mu_1 = 7.55$. The uncertainty in the average (of 7.36 ± 0.19) is 2.6%, and could be attributed to an oversimplification in assuming the evolution of initial Pb in a single stage. Specifically, the higher μ_1 from $^{207}Pb/^{204}Pb$ indicates that in its evolution (in multiple stages), the initial experienced an early period (less than the 0.8-Ga interval) with μ greater than the calculated μ_1. As a result, the initial contains excess ^{207}Pb, related to the higher production rate of the isotope in early times. In section 5.3 it is suggested that before the formation of the ancient terrestrial reservoirs, the differentiating material had experienced strong Pb loss (relative to U) in the first 0.06 Ga, resulting in a more evolved Pb than the accepted primordial of Tatsumoto et al. (1973). This conclusion is in a qualitative accord with excess ^{207}Pb in the inferred initial of the Amîtsoq gneisses.

5.2.5.2. What if the 4.42-Ga age is real? Implicit in the ongoing controversy about the age of the Amîtsoq gneisses is a discounting of the survival of an ancient crust much older than ~3.9 Ga. The prevailing view is that the earth's evolution records of the first 5×10^8 yr were lost because of efficient resurfacing of the planet early in its history (e.g., Bowring and Housh, 1995). Thus for the Amîtsoq gneisses, the issue has centered on two narrower options: (1) The complex contains rocks of multiple ages, implaced in short-duration magmatic events between 3.850 and 3.550 Ga (e.g., Nutman et al., 1996,

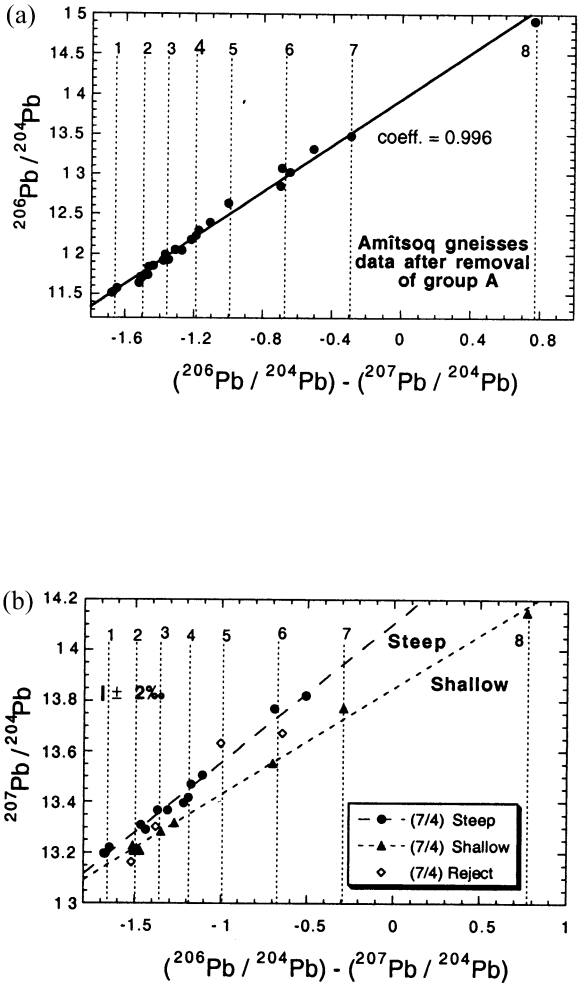

Fig. 20. (a) Differential $^{206}Pb/^{204}Pb$ correlation for the data shown in Figure 18 after subtraction of group-A samples. The axes are extended to include the six most radiogenic samples. (b) Differential $^{207}Pb/^{204}Pb$ correlation of same data. Note resolution into two trends labeled "Steep" and "Shallow." Four points may be aberrant (open circles).

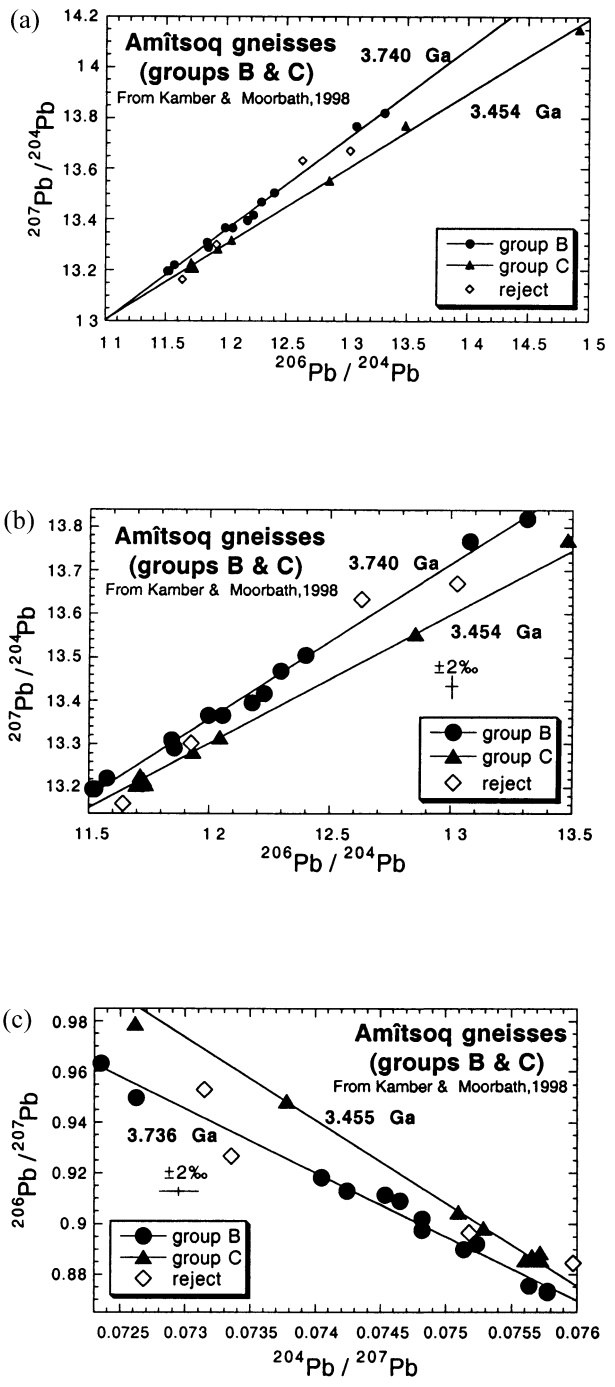

Fig. 21. (a) Amîtsoq's left-over data (after removal of data defining line A in Fig. 18(1) appear to fall on two lines, labeled B and C, which intersect at a point possibly corresponding to initial Pb of the system (see section 4.2). (b) Same data (except one) on expanded scales of a type I diagram. (c) Same data on a type III diagram. Conventional calculation yields exactly the same ages but with ±0.080 and ±0.059 Ga for lines B and C, respectively.

2000), and (2) the rocks formed primarily in a single magmatic event at 3.600 to 3.650 Ga (Kamber and Moorbath, 1998). The first scenario is based on a range in the zircon ages. The second is based on a model-influenced interpretation of the whole rock data, from which a single age is inferred, and older zircons are considered inherited.

In this section I consider the possibility that the 4.42-Ga age is real. That the other clock-systems do not show the 4.4-Ga age is not surprising. The conventional Pb-Pb method did not show it either, despite being uniquely dual. Without the differential correlation procedure and the ability to sort out samples, the effect might have remained masked. In this connection one should mention that Harper and Jacobsen (1992a) reported the existence of excess ^{142}Nd in ~3.8-Ga metasedimentary rock from Issua, Greenland. This was attributed by them to the derivation of this rock from a mantle reservoir that was depleted in Nd (relative to Sm) at a time earlier than 4.3 Ga (^{142}Nd is produced by the decay of the now extinct ^{146}Sm [half-life = 0.103 Ga]). So far, however, no excess ^{142}Nd was detected in any sample from any other location (Goldstein and Galer, 1992; Harper and Jacobsen, 1992b; Sharma et al., 1996).

As to the argument against the 4.4-Ga age on the basis of its absence in zircons, it must have lost some of its edge. While

this work was in review, an article by Wilde et al. (2001) reporting an age of 4.4 Ga for a spot in a zircon (Jack Hills, NW Australia) appeared in the literature. I have looked at the data on ancient zircons with some care and tentatively arrived at views which may be considered additions or alternatives to the conventionally accepted ones. These are discussed in section 5.4.

5.3. Sources of Crustal Rocks

Consistent with the Pb isotope systematics, the intersection of a number of isochrons at a single point may indicate the derivation of their rocks from a single reservoir. The present-day composition of that reservoir is given by the point of intersection. Assuming the applicability of this algebraic deduction to terrestrial rocks, Stacey and Kramers (1975) arrived at an average composition of $^{206}Pb/^{204}Pb = 18.70 \pm 0.1$ and $^{207}Pb/^{204}Pb = 15.64 \pm 0.04$ for what they termed "modern terrestrial lead" (MTL). Subsequently, it was observed that most of the Ocean Island Basalts (OIB) lie to the right of the geochron (that is, an isochron passing through the primordial Pb isotopic composition, PAT, and having a slope yielding the age of the Earth). This indicates enrichment in U (relative to Pb) in the sources of OIB. The apparent absence of complimentary depleted terrestrial sources gave rise to the so-called "Pb paradox."

With its potential of allowing the filtration of Pb isotopic data, the concept of synchronism (section 2) was applied to a large body of data on crustal rocks (including those used by Stacey and Kramers, 1975). The results (not detailed in this work) indicate multiple intersections, covering a wide range of discrete compositions, suggesting that MTL is but one reservoir among many. Some isochrons intersect at low values for $^{206}Pb/^{204}Pb$ and $^{207}Pb/^{204}Pb$, a condition consistent with their derivation from a U-depleted reservoir. If so, then the so-called "Pb paradox" may have no existence outside the imagination.

One tentative indication to the existence of a U-poor reservoir (let's call it reservoir I) is given by the intersection of the Pb-Pb isochrons of the Vikan gneiss of Norway (older event), the Vredefort basement of South Africa, and the Lewisian gneiss of Scotland (all discussed in section 5.2). As Figure 22 shows, the intersection of these lines is at $^{206}Pb/^{204}Pb = 14.69$ and $^{207}Pb/^{204}Pb = 14.78$, values which are far less evolved than MTL mentioned above (this section). Another potential indication to a U-poor reservoir (let's call it reservoir II) is from the intersection of the lines of: the Vikan gneiss (younger event), Beartooth Mountains of Montana and Wyoming, USA, and Broken Hill of Australia. The result is shown in Figure 23, and indicates $^{206}Pb/^{204}Pb = 16.15$ and $^{207}Pb/^{204}Pb = 15.38$.

On the basis of the above, one may be persuaded to assume the actual existence of U-depleted reservoirs within the earth. It could be argued that in view of the evidence of disturbance and superimposed events in ancient terrain, the specifics of the fine resolution shown may be open to some doubt. However, the fact remains that the isochrons shown infer reservoir-values far less radiogenic than MTL.

The reservoir values in Figures 22 and 23 as well as an average of both, indicate a peculiarity in the early Earth's evolution: subtraction of Cañon Diablo primordial Pb (Tatsumoto et al., 1973) results in the high values of *($^{207}Pb/^{206}Pb$),

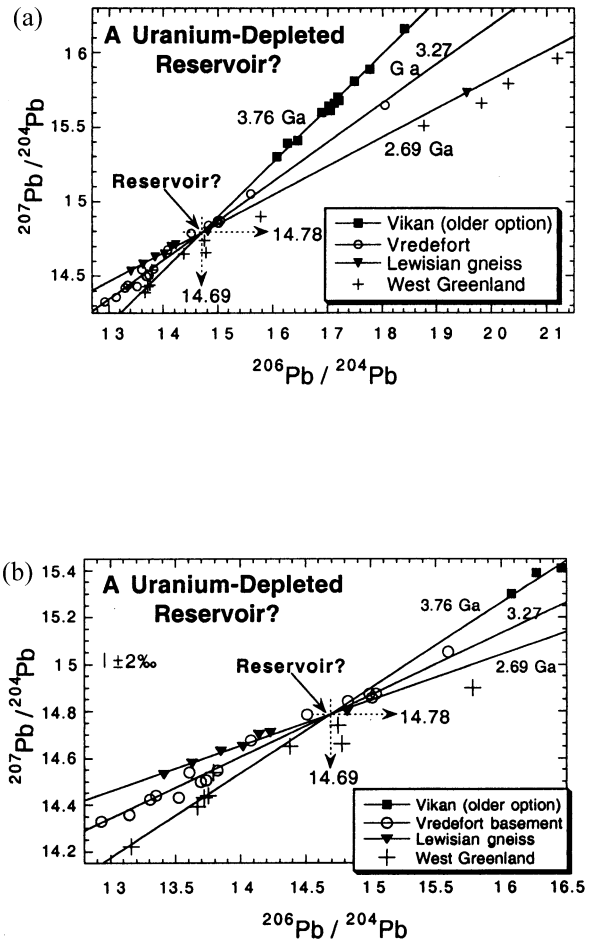

Fig. 22. (a) Filtered data of three isochrons for rocks from widely separated places (Vikan gneiss, Norway; Vredefort dome, South Africa and Lewisian gneiss, Scotland), result in their intersection at a single point. This may indicate derivation of the rocks from a single source. (b) An expanded section of (a). Note apparent affinity of the unfiltered data of West Greenland (data of Black et al., 1973) with this group of rocks.

equaling 0.833 for reservoir I, and 0.743 for reservoir II. Respectively, the corresponding calculated single-stage ages are 4.98 and 4.82 Ga, an indication to the inapplicability of the model. Variations of the two-stage model of Stacey and Kramers (1975) result in inconsistency between the results from $^{206}Pb/^{204}Pb$ and from $^{207}Pb/^{204}Pb$, in a manner indicating excess ^{207}Pb. For the two examples under consideration, the results from the two isotope systems are reconciled by a three-stage calculation, in which $\mu_1 = 30$ for a first stage (duration 4.560–4.503 Ga) and $\mu_2 = 7.0$ for a second stage (duration 4.503–3.760 Ga). For reservoir I, $\mu_3 = 4.2$ for the third stage (3.760 Ga to the present). A guidance from the model of Stacey and Kramers (1975) provided the parameters of the second stage in the present calculation. The choice of 3.76 Ga (rather than 3.70 Ga of Stacey and Kramers, 1975) was dictated by the necessity that the source cannot be younger than its oldest isochron (see Fig. 22). Reservoir II could be derived from reservoir I, where with the same $\mu_3 = 4.2$, the third stage duration ended at 3.39 Ga (age of its oldest isochron, Fig. 23).

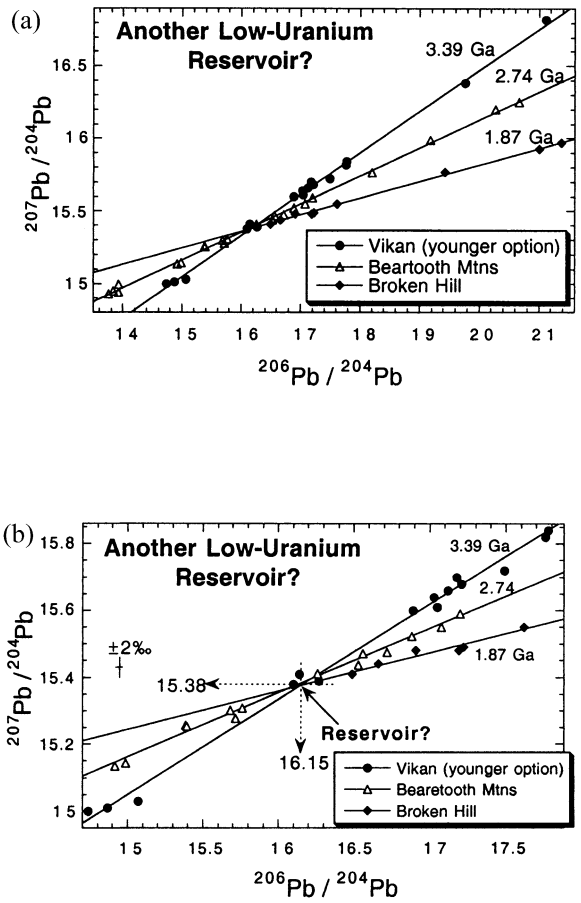

Fig. 23. (a) Intersection in a single point by another three isochrons: The Vikan gneiss of Norway (younger isochron), Beartooth Mountains (Montana and Wyoming, USA) and Broken Hill (Australia). For Beartooth Mountains (Wooden and Mueller, 1988), 91% of the data (31 out of 34 data points, not discussed in this work) form a line corresponding to 2.74 ± 0.01 Ga (error based on all three Pb-Pb diagrams).(b) An expanded portion of (a) clearly showing the point of intersection.

Here calculations from $^{206}Pb/^{204}Pb$ and from $^{207}Pb/^{204}Pb$ concur on $\mu_4 = 6.30$ for the fourth stage duration (3.39 Ga to the present).

Thus in addition to indicating the existence of U-depleted reservoirs the data as presented specify the timing of a very early episode of severe ^{204}Pb depletion (relative to U). Assuming the general validity of the modification introduced to the well-reasoned model of Stacey and Kramers (1975), the alleged Pb depletion appears to have taken place within the first 6×10^7 yr of the earth's existence. The severity of the depletion in the first stage may be masked in the more evolved sources: for example, the same three-stage calculation could be applied to MTL with $\mu_1 = 10$.

It is perhaps worth noting that MTL lies distinctly away to the right of the (single-stage) geochron, thus its Pb isotopic composition cannot even come close to representing an average for the Earth, more than the depleted sources, which lie closer to the geochron (no figure). Implicit in the ubiquitous imprinting of the "exterior" of the globe with the rather radiogenic MTL, is the anticipation of inaccessible U-depleted reservoirs, for which I tentatively suggest some evidence is provided here.

Assigning a lower limit to the age of a reservoir on the basis of its oldest isochron, and associating inaccessibility of low μ with depth of its sources, one might infer on the basis of Figure 22 a deep mantle convection for the first 0.8 billion years of earth's existence (4.56–3.76 Ga), followed by a shallower mantle convection 3.4 Ga ago, when reservoir II was formed (Fig. 23). Related to this view of decreasing depth of convection with time (see Sun and Hanson, 1975) would be a question regarding the mechanism by which μincreases with time. In accord with the phenomenon is Pb loss (as ore deposits) from the shrinking accessible silicate reservoir, but this is a minor contributing factor.

5.4. The Zircon Wilderness

Having assumed the validity of the 4.42-Ga age in one of the scenarios for the Amîtsoq gneisses (section 5.2.5.2), I attempt here to reconcile this assumption with the data from zircons. This requires showing that some of the 3.8- to 3.9-Ga zircons are potentially much older. This is possible if radiogenic Pb of the duration 4.4 to 4.0 Ga was almost (but perhaps not quite) completely lost from the ancient zircons. In this connection I take note of the fact that 40% of radiogenic ^{207}Pb (and 19% of ^{206}Pb) was produced at that interval. Could the ancient zircons, formed within this period, have sustained consequential radiation damage?

According to Pidgeon et al. (1966), other factors being equal, a zircon's susceptibility to Pb loss is proportional to the degree of its radiation damage. On the other hand according to Murakami et al. (1991) and Nasdala et al. (1996), the damage resulting from recoil during α-decay and fission are only of minor importance. It is my conjecture that major Pb loss was mediated by radiation damage in association with early thermal and intense bombardment events, in addition to possible hydrothermal processes.

If the Pb loss was $> 90\%$, then the U-Pb data of these zircons would cluster today close to the concordia curve, at regions of much younger ages than 4.4 Ga. The superposition of metamorphism on top of that, in addition to Pb loss in recent times, further adds to the complexities of the patterns of dispersion and often to the deception of apparent younger ages. This is because such loss, superimposed on sample clustering close to concordia downward from the 4-Ga mark, creates trajectories that are at shallow angles from the horizontal, which creates a false sense of convergence on a younger age (see Fig. 24a).

5.4.1. Commonness of a 4.4-Ga Terrestrial Crust?

Making its first appearance in an abstract three years ago, the idea of a 4.4-Ga terrestrial crust had the status of a heresy because the 4.4-Ga imprint was inferred via a new methodology, which was introduced at the same time (Tera, 2000a, 2000b). The subsequent report on a concordant (U-Pb) datum of the same age, for a spot in a fragment of a detrital zircon (Wilde et al., 2001), provided a glimpse of evidence that is perhaps less disputed. The emerging reality is still blurred, and has yet to sink in, not to mention be put in the physical context of an evolving terrestrial crust. In this report I provide further

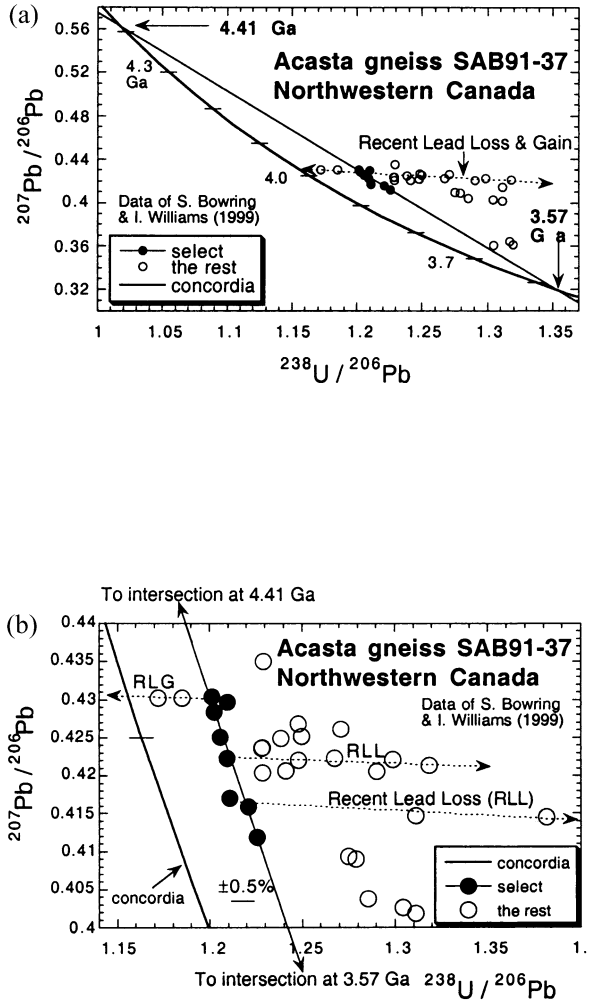

Fig. 24. (a)"SHRIMP" data on individual zircons (from an Acasta gneiss) with Pb-Pb ages > 3.5 Ga. Note general trend of dispersion at a wide angle relative to concordia. This may suggest recent U-Pb mobility. (b) Within the dispersion field some data points (filled circles) appear to define a coherent linear trend (5% range in 207/206), indicative of a cord that intersects concordia at 3.57 and 4.41 Ga.

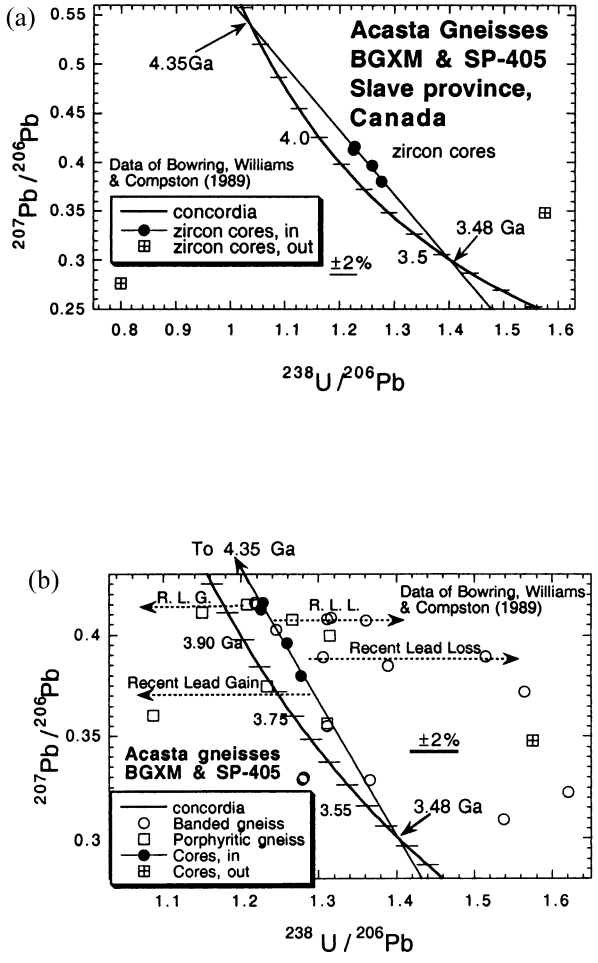

Fig. 25. (a) U-Pb data by SHRIMP on six (unaltered?) zircon cores from two Acasta gneisses. Two cores deviate from a 3.48 to 4.35 Ga cord, which the other four appear to define. (b) The rest of the individual-zircon data scatter, possibly in events which may include recent Pb loss and gain (dotted arrows). Thirty-five percent of the data points fall on the cord.

"evidence" to the existence of such a crust in multiple places, vastly separated from each other around the globe. The use of quotation marks is to indicate the equivocal quality of the evidence at this stage. These may be taken as the elements of a hypothesis posed to challenge our acumen to a concrete resolution.

5.4.1.1. Western Slave province, Canada. The SHRIMP (Sensitive High-Resolution Ion Microprobe) U-Pb data on individual zircons, in the Acasta gneiss SAB91-37 (Bowring and Williams, 1999) are shown in Figure 24. For the sake of the specific search for an ancient imprint, data with Pb-Pb ages < 3.5 Ga were excluded. A general, apparently dominant, and nearly horizontal trending is obvious. This pattern is not inconsistent with recent extensive Pb mobility (mostly loss). If present, vestiges of the ancient first-stage Pb (ancient upper intersection) may be identifiable only in samples, which did not experience isotopic disturbance throughout the second stage duration (i.e., undisturbed lower intersection), including the apparently pervasive recent Pb mobility. Out of some 30 samples of gneiss SAB91-37 on the horizontal trend (Fig. 24a), eight are tentatively identified as potentially preserving an ancient profile. This tenuous profile indicates upper and lower intersections with the concordia curve at 4.41 and 3.57 Ga, respectively. On an expanded scale in Figure 24b the eight ancient-profile data are seen to appear coherently clustering around the 4.41 to 3.57 Ga cord, in isolation from the rest of the data. For a three-stage evolution (free of recent mobility) the upper intersection is a lower limit.

The above observation seems supported to a degree by the data on six unaltered cores of zircons from two other Acasta gneisses, from the Slave province, BGXM and SP-405 (Bowring et al., 1989). The data are shown in Figure 25. Four of the cores form a line, which intersects the concordia curve at 4.35 and 3.48 Ga. In the author's opinion, this coincidence may not be accidental, and may indicate once wide-spread existence of an ancient crust (~4.4 Ga old) in Western Canada.

In contrast to gneiss SAB91-37 (Fig. 24), the U-Pb data of Acasta gneiss SAB94–134 (Bowring and Williams, 1999) scatter and overlap within a large dispersion field. However, influenced by the possibility that an ancient crust did once prevail in that region, one may realize that fully 50% of the data cluster (within ±1.5% errors on the x-axis) around a line which intersects the concordia curve at 4.32 and 3.62 Ga (no figure is shown).

5.4.1.2. Western Australia. In Figures 26 and 27 are shown the pioneering work of Froude et al. (1983) and Compston and Pidgeon (1986), applying the ion-microprobe SHRIMP technique to individual detrital zircons from Mt. Narryer and Jack Hills belt, Western Australia. The original authors (Froude et al., 1983) were impressed by the concordance (within large errors) of three data points in the region between 4.1 and 4.2 Ga. On the basis of the directly determined $^{207}Pb/^{206}Pb$ they assigned these as minimum ages of the zircons. My attention is drawn to the seven spot-analyses of grain 34 (circles): Within error bars of ± 0.5%, four of the points define a line (filled circles), which has an upper intersection with the concordia curve at 4.48 Ga! Is this an accident, or a greatly significant result, which also indicates that the assigned U/Pb errors are often exaggeratedly larger than the actual experimental errors?

The data of Compston and Pidgeon (1986) on Jack Hills zircons appear to support the second possibility, namely the existence of a diagnostic vestige of an ancient crustal imprint in the zircons from Western Australia. In Figure 27a, fully 55% of the data cluster around a cord which has an upper intersection with the concordia at 4.4 Ga. Furthermore, the cluster appears to stand well separated from the rest of the data which are more dispersed. Interestingly, the evidence to antiquity in this data set appears largely independent of the stringency of filtration. Thus if only the six most deviant samples are filtered out, the remaining data (67%) will define a cord which intersects concordia at 4.62 Ga (Fig. 27b). While this excessively old age does not represent a proof to antiquity, it could be thought of as being due to a minor adulteration of an original profile, causing an overshooting to the older age. In general then, the profiles in Figures 27a and 27b appear in accord with the recent discovery of Wilde et al. (2001) of a Jack Hills zircon with an age as old as 4.404 Ga. It seems indeed conceivable that an ancient (4.4 Ga) crust prevailed in Western Australia as well.

Concerning the experimental errors in the SHRIMP-data, I note occasional striking reproducibility. For example in the work of Williams et al. (1984), on a zircon from Mount Sones, Antarctica, the $^{238}U/^{206}Pb$ of the three measurements in a single spot in one session was reproducible within ±0.5%. One of two measurements in the same spot in another session agreed with the earlier average within 0.7%; the other was deviant by 6% (These are all the measurements done on spot 1 of grain 7). Similarly, two thirds (10 out of 15) of the "reconnaissance" U-Pb data on a single zircon by the same workers fall on a single line within ~1%.

5.4.1.3. Intermediate cases in Antarctica and West Greenland. It is reasonable to assume that the earth was subject to the same cataclysmic bombardment which the moon seems to have experienced, and which terminated ~3.9 Ga ago (see for example, Tera et al., 1974). Unlike the moon, the earth's extended differentiation can result in a range of lower intersections with concordia at values ≪3.9 Ga. Thus ancient zircons, >3.9 Ga (which experienced the cataclysm, in addition to subsequent metamorphism) may have evolved their Pb in a minimum of three stages.

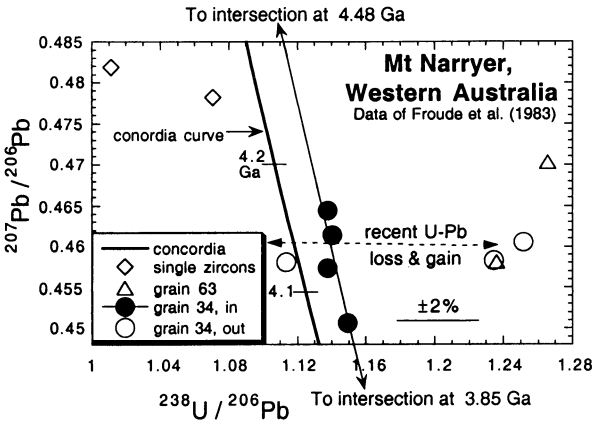

Fig. 26. U-Pb data on detrital zircons from Mt. Narryer, western Australia. Of the seven spot analysis on grain 34 (circles), four appear to fall on a cord that intersects concordia at 3.85 and 4.48 Ga. The age of the lower intersection suggest approximation to Pb evolution in two stages.

The effect of a strong third event (or higher order) on samples deficient in first-stage Pb, is to shift the position of their upper intersection further downward. This condition (or an equivalent to it) may apply to the zircons of Antarctica (Black et al., 1986), shown in Figure 28a. Even in cases where the dispersion is most severe and association with younger concordia-ages is "apparent," vestiges of the ancient heritage may still be inferred, albeit tenuously. The case of the Akilia island of southern West Greenland (Nutman et al., 1996) may serve as an illustration. In Figure 28b, 70% of the data are shown to fit inside a parallelogram the width of which corresponds to ±5% in the $U/^{206}Pb$ ratio. The lengthwise median of the parallelogram is part of a cord, which intersects the concordia curve at 4.23 and 3.4 Ga. On that cord fall 23% of the shown data (filled circle). The assumption here is that these are probably the least disturbed of the zircons shown, thus extensive spot analysis in them (as done in Wilde et al., 2001) may reveal aspects of an ancient imprint.

5.5. A Single Accurate Age for the (Parent of) Ordinary Chondrites?

It was concluded that the ordinary chondrites' data (of Göpel et al., 1994) fall on a line in a Pb-Pb diagram, indicating an age of 4.553 Ga for their parent body (Tera et al., 1997). Here, the chondrites' linear array (data of Göpel et al., 1994, and Unruh, 1982) are re-examined in the light of the concept of isotope synchronism. Because the age is nearly synchronous, no filtration through the differential correlation procedure is needed. In the conventional (type I) diagram, the data are co-linear with both the blank and primordial Pb (no figure shown). This

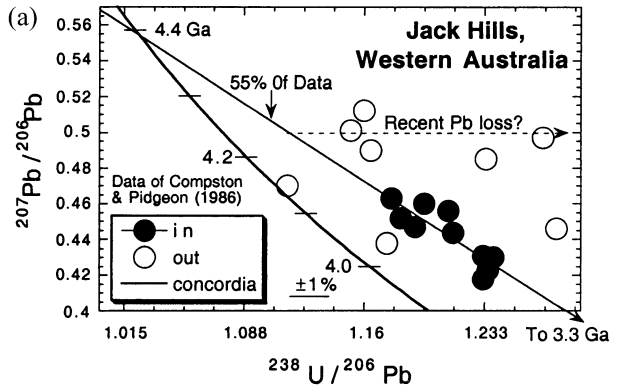

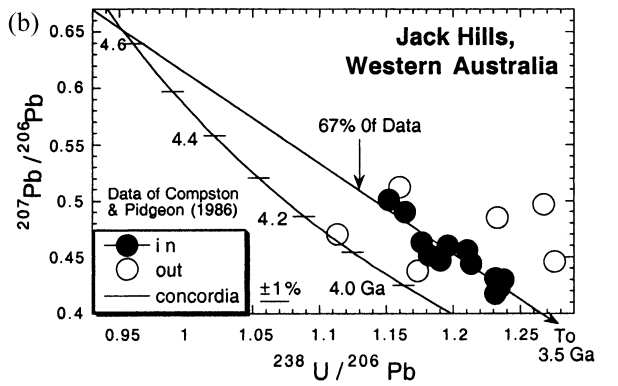

Fig. 27. (a) U-Pb data on individual zircons from Jack Hills, western Australia. Fifty-five percent of the data points (filled circles) appear compatible with a cord having an upper intersection with the concordia curve at ~4.4 Ga. (b) A cluster containing 67% of the data yields an upper intersection at 4.62 Ga. The excessively old age may be an artifact resulting from including in the profile "extraneous" samples which experienced recent Pb loss (compare with [a]). The same cord is obtained with 78% of the data (not shown).

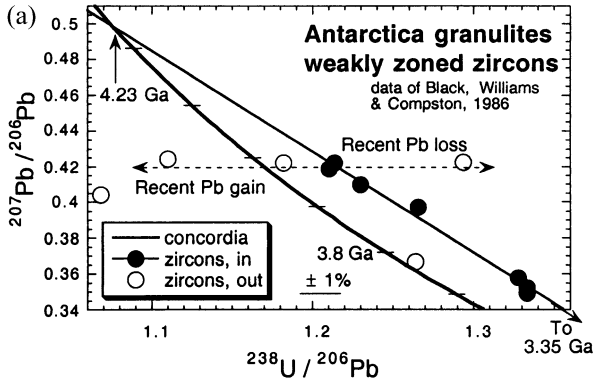

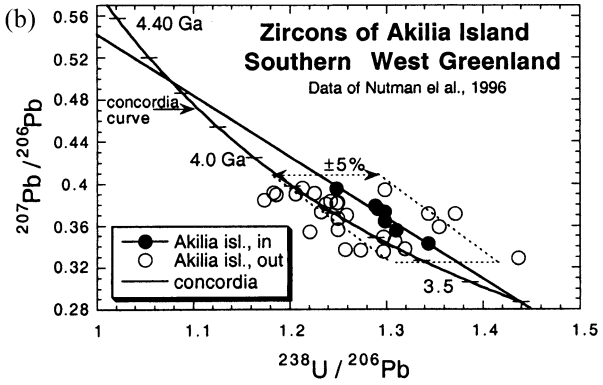

Fig. 28. (a) Zircons of Antarctica granulites appear to show evidence of an upper intersection at ≪4.4 Ga. This could be the result of more extensive Pb loss at a first stage (say 4.55–3.9 Ga period) followed by more recent metamorphism. (b) A tenuous proposition that despite severe disturbance, spot analysis on some individual zircons (like those of the filled circles) may reveal a modified (possibly ~4.4 Ga) ancient history.

circumstance disqualifies type I correlation in the search for the condition of synchronism. In its place a type III correlation is used (Fig. 29b), where the blank falls off the line. In both figures (Figs. 29a and 29b) the best fit line misses PAT into a "forbidden" region. Such an artifact is in all probabilities caused by terrestrial Pb contamination, which would also disperse the data.

If contamination is the only cause of deviation from PAT and the only source of dispersion, then the data would fall inside a dispersion field defined by three end-members: PAT, the blank, and in-situ decay Pb, as is indicated by the partially shown triangle in Figures 29a and 29b. As seen in either figure, three data points fall distinctly outside the field, and another three fall just outside its borders. This indicates additional causes for the observed dispersion, as for example open-system behavior and/or multistage evolution. Inside the triangle, four additional points appear dispersed. Filtering out the above mentioned 10 deviant data (out of a total of 31 data points for 15 meteorites), the results are shown in Figures 29a and 29b, to yield a nearly perfectly reproducible age of 4.555 Ga which is synchronous within $\pm 3 \times 10^5$ yr.

It should be pointed out that most of the deviant data (7 out of 10) are repeat analyses for otherwise well behaving meteorites. Thus out of 15 meteorites studied only 3 (or 20%) are deviant. This strict and encompassing synchronism cannot be an accident. The 4.555 Ga age is taken to be the date of possibly one of the earliest differentiation events in the Solar System. This date is also a lower limit to the age of formation of the parent body of the ordinary meteorites.

This view discounts attaching direct temporal significance to the range of ages (4.56–4.50 Ga) for phosphates in these meteorites (Göpel et al., 1994). Basically, these are model ages of individual minerals.

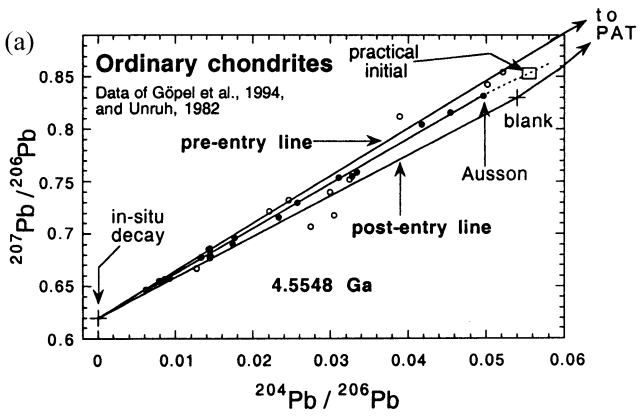

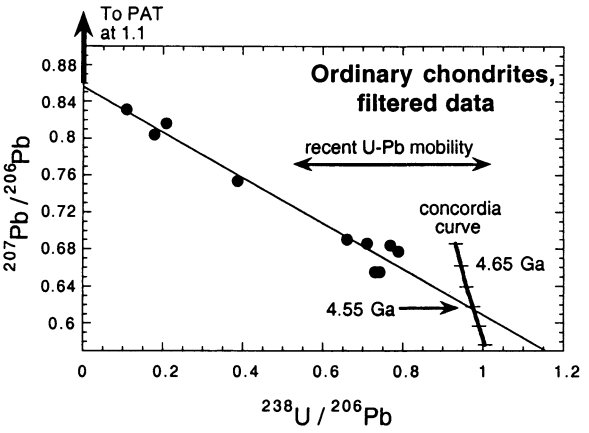

Fig. 30. Ordinary chondrites' filtered data define a line on the concordia diagram that intersects the y-axis at a point which is far below the PAT value. Conclusion: ^{204}Pb in the samples is overwhelmingly of terrestrial origin, perhaps acquired as the meteorites entered the earth's atmosphere (see text). Data from Göpel et al. (1994).

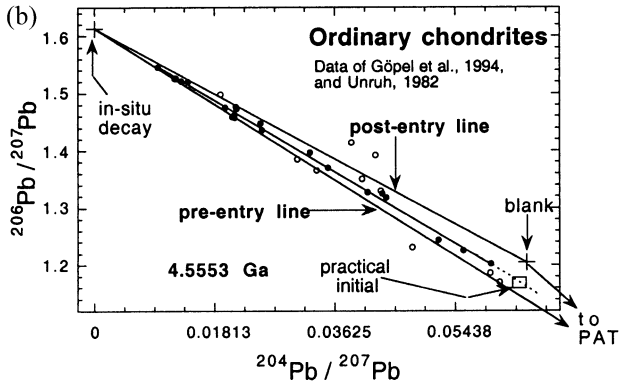

Fig. 29. (a) The dispersion field of the ordinary chondrites (L5 and 6 and H; Unruh 1982; Göpel et al., 1994) is a triangle (partially shown on type II diagram), the end members of which are: PAT, blank, in-situ decay. Samples outside the field are most disturbed. Majority of the data (70% of the points, 80% of the meteorites, solid dots) define a best-fit line inside the field corresponding to 4.555 Ga age. (b) Same data plotted on type III diagram, indicating that the age is synchronous within $\pm 3 \times 10^5$ yr.

5.5.1. Initial Pb of the Ordinary Chondrites

The high degree of synchronism exhibited by the filtered data of the ordinary chondrites is an indication to the apparent absence of system errors (section 2.1). Consequently, the Pb of all these samples is made of the same two components: (1) in-situ decay Pb, which evolved in a single stage and (2) inherited initial Pb of a singular composition. The isochron in Figure 29 shows that singular component not to be PAT. This conclusion is more visible on the modified concordia diagram for some of these samples (Fig. 30) where it is seen that the U-Pb isochron intersects the y-axis at ($^{207}Pb/^{206}Pb$) = 0.855 instead of the PAT value of 1.1. This was indicated earlier on the basis of all the data (more scatter), without the benefit of filtration (Tera, 1983; Tera and Carlson, 1999).

The limited scatter in the filtered data in Figure 30 indicates that recent U-Pb mobility is not a major factor in the exhibited range of distribution. Thus the intercept value in Figure 30 may be translated to a corresponding "practical initial Pb" in Figures 29a and 29b, shown as a small square at the tip of the best-fit line. The values inferred are $^{206}Pb/^{204}Pb$ = 18.1 and $^{207}Pb/^{204}Pb$ = 15.5. These values fall within the wide range of initial Pb values (e.g., $^{206}Pb/^{204}Pb$ = 16.2–18.3 for L5 and L6) inferred from the troilite separates of L chondrites (Unruh, 1982). Although narrowly defined, the trouble with the "initial Pb" inferred here, however, is that it is far too radiogenic, that it would evolve in ~4.5 Ga from PAT. Additionally, its corresponding μ is 8.7, which is similar to that of MTL. Thus, a plausible explanation of the patterns in Figures 29 and 30 is

1. The initial lead in ^{204}Pb-"rich" chondrites is overwhelmingly of terrestrial origin; perhaps permeated the rocks as they entered the earth's atmosphere. If one assumes $^{206}Pb/^{204}Pb$ = 18.5 for the terrestrial component, then it must contribute ~95% of the Pb in the composite make-up of the "practical initial" shown in Figures 29a and 29b. On the basis of his U, Th and Pb analyses of whole-rock and troilite separates from seven L chondrites, Unruh (1982) suggested that the excess radiogenic Pb in chondritic meteorites is largely due to terrestrial contamination before analyses.
2. Applying the practical initial value to Ausson, the least radiogenic meteorite defining the line in Figure 29a (or Fig. 29b), one calculates a meteoritic ratio of $^{206}Pb/^{204}Pb$ = 49 for this meteorite instead of the literature value of 20. A similar calculation for the most radiogenic sample, Knyahinya, yields a value of 287 instead of the reported value of 161.
3. However, it is possible that the most radiogenic samples are relatively free of the terrestrial component. As such they belong to the "preentry line" in Figures 29a and 29b, while the affinity of the less radiogenic samples is shifted to the "postentry" line. Because of the mutual convergence of the two lines toward the in-situ point, resolving the more radiogenic data into two categories is not possible.
4. The compactness of the above mentioned dispersion field helped preserve the linearity of the data and the essential

validity of the determined age. Correlated filtration of deviant samples is another important factor. This case is a demonstration of the fact that in Pb-Pb dating, the geometry of the field of dispersion can be more important than the magnitude of contamination.

5. The 11 most radiogenic samples are essentially compatible with PAT, with which they constitute a line corresponding to 4.552 Ga (no figure), a further indication that the obtained synchronous age (Figs. 29a and 29b) may indeed be valid within a few 10^6 yr.

5.5.2. Comparison With Allende Inclusions

Assuming the validity of PAT as the initial Pb composition of the Solar Nebula at the time of planetisimal accretion, no valid Pb-Pb isochron (of Solar System materials) should plot to the right of PAT, on a type II Pb-Pb diagram. As shown in Figure 10b (discussed in section 4.3.1), the Allende inclusions' Pb data (of Chen and Wasserburg, 1981) define a line the extension of which falls far to the right of PAT, a forbidden region. Discounting on the basis of good evidence (by Chen and Wasserburg, 1981) a variability in U isotopic composition, this "violation" has one of two explanations: (1) Allende inclusions predate accretion and thus contain initial Pb that is more primitive than PAT, or (2) the line is an artifact affected through terrestrial Pb contamination.

The plausibility of the latter scenario appears strengthened by the fact that the point of MTL (mentioned in section 5.3) which is similar to the blank, falls on the Allende line. However, close examination of the diagram reveals a state of stringent linearity inconsistent with the expected dispersion within a three-component field; thus Tera and Carlson (1999) argued for the possibility that the line defined by the inclusions is a bonafide isochron independent of MTL. Another point to add here in support of this view is the geometric impossibility of shifting the three most radiogenic Allende inclusions (filled circles in Fig. 10c) from the "pristine line" to the "translocation line," via mixing with MTL. The dictum derives from the fact that a contamination-translocation line is an artifact in which the higher intercept value is *inferred*. Such inference becomes possible only from translocation of data points falling to the right of the Quasi Dual Point (see Fig. 10c). If present, data points falling to the left of QDP have a contamination trajectory that lags behind the affected rotation, and should cause dispersion instead of confirming the line (as the case on hand appears to show).

A third scenario is permitted by the data under consideration: As shown in Figure 10d, they seem to fall in two groups, one of which is consistent with PAT at a younger age of 4.488 Ga, and the other suggesting a "PrePAT" initial, and an older age of 4.568 Ga. Although this scenario does not appear inconsistent with the analytical precision of the data, elaboration on it may not be fruitful until the Pb isotopic composition of the inclusions is determined at the newly attained level of higher precision. At present, ambiguity prevails.

5.6. Ocean Island Basalts (OIB)

It may seem on the surface that the concept of synchronism could not be applied to Ocean Island Basalts (OIB) because these are bodies, which were brought to the surface recently in a molten condition. Although long-term isolation of magma reservoirs has long been accepted and evidence for it been provided (see for example Sun and Hanson, 1975; Brooks et al., 1976; Hart, 1984; Zindler and Hart, 1986), one might envision the molten state as inducing mixing and open-system behavior, a condition which may strongly disturb or erase preexisting isochrons. In addition, having a convecting mantle as the source adds a potential eraser of whatever vestiges of isochronism that might have survived for a while. On top of that is the possibility of assimilating exogenous materials along the pathway of a given magma. On the other hand these and other obstacles to the application of synchronism to OIB need not be completely preclusive, because the concept is applied to data that are filtered. Thus the only criterion of suitability is the survivability of some samples. However, because the singular measure of survivability is the defining of a line that is reproducible in various Pb-Pb diagrams, such a line could result from the accidental alignment of a few points in a chaotic dispersion field. To guard against this, a line based on a few data points (say, $<$20% of a "representative" population) may be viewed with suspicion.

With the above in mind, Pb data on five ocean islands were filtered. They were found to produce, each, what appears to be a temporally synchronous line. However, only two with large bodies of data (Hawaii and Iceland) are discussed here. Although not prompted by the concept of "mantle isochron" put forward by Brooks et al. (1976), the effect discussed here appears as a fine-scale extension of it.

5.6.1. An Iceland Isochron?

The Pb data on Iceland (by Hanan and Schilling, 1997) are shown on all three age-producing diagrams (Fig. 31) and yield ages ranging from 1.1 to 1.8 Ga, clearly indicating pervasive open-system behavior. On the conventional diagram (Fig. 31a), the field of Iceland data reveals a scatter from the best-fit line which is dominated by large shifts (often in the percent range) along the x-axis, accompanied by $<\pm 1.5‰$ shifts along the y-axis. This pattern is characteristic of disturbance in very recent times ($<$1 Ga), where the production of ^{207}Pb is negligible. On type III diagram (Fig. 31c), this fractionation scenario results in the opposite effect, i.e., major shifts along the y-axis associated with minimum shifts along the x-axis.

Under a condition where ^{207}Pb production approaches zero, U-Pb fractionation amounts to gain-loss of ^{206}Pb alone. This condition would result in shifts on the x-axis and y-axis of the type II diagram, which are uniformly correlated and non-dispersive. In other words, data of the disturbed samples would merely slide up and down along the length of the isochron defined by the closed-system data; i.e., very recent disturbances ($\ll$1 Ga) scatter the data on types I and III diagrams, but may not register on type II. This appears to be the case of the Iceland data, where it is seen that the scattered data in Figures 31a and 31c (coefficient of correlation $\sim$ 0.7) are falling coherently on a line in Figure 31b (coefficient = 0.995).

On the basis of the above analysis and rationale, I tentatively concluded that

1. The date of 1.06 Ga in Figure 31b may be a close approximation to the true age of the source of Iceland basalt

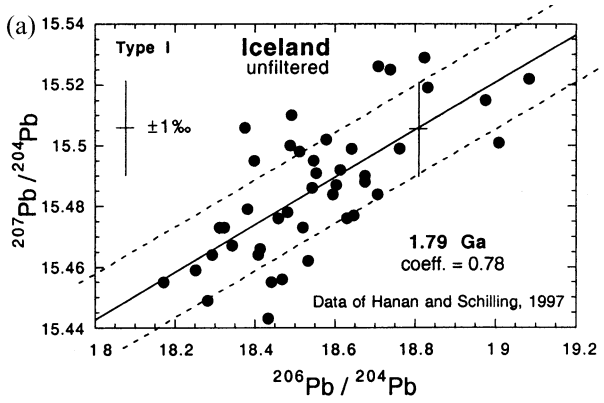

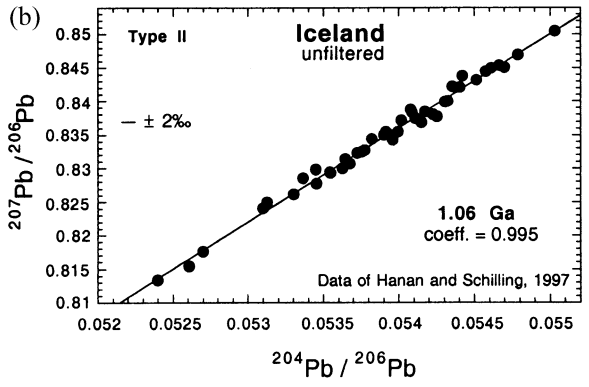

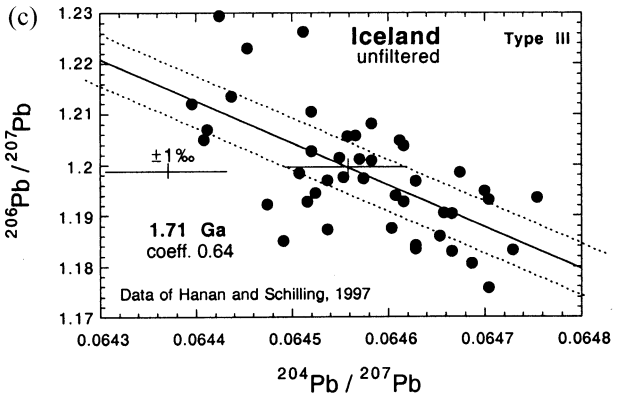

Fig. 31. (a), (b) and (c) The patterns of Iceland data (Hanan and Schilling, 1997) indicate primary control by loss-gain of ^{206}Pb alone. This could result from a very recent disturbance. Because of correlated trajectories in Figure 31b such disturbance may not affect the age in this diagram.

2. This ~1.0-Ga system was disturbed in very recent times ($\ll$1 Ga), which resulted in extremely small gain-loss of ^{207}Pb.
3. Because of the conclusion in point (2), filtration of the data by the differential correlation method must be carried out on an ultra-fine scale.

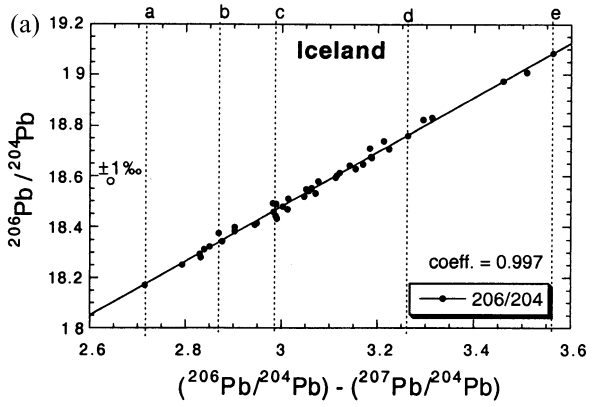

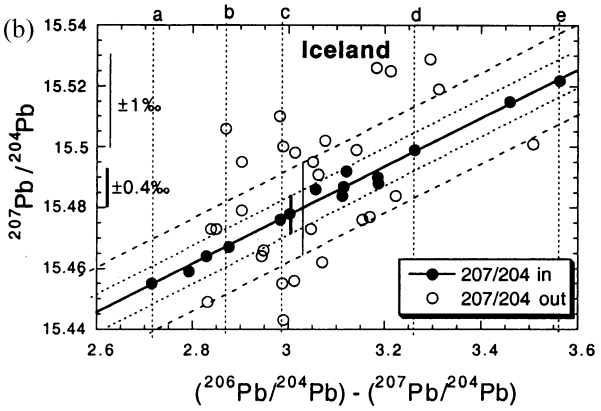

Fig. 32. (a) and (b) Consequential disturbance of the Iceland data on the per mill level in ^{207}Pb/^{204}Pb, requires filtration on the sub–per mill scale. Filtering on the 0.4‰ level results in a synchronous age defined by 35% of the data points (see Fig. 33).

The differential correlations for Iceland data are shown in Figure 32. Limited trial and error revealed that filtering at the 0.4‰ level (see Figs. 32a and 32b) results in a synchronous isochron of 1.058 ± 0.0006 Ga (see Fig. 33). This age is indeed the very same age obtained from the *unfiltered* data on type II diagram (Fig. 31b). It thus seems safe to conclude that the line defined by the Iceland data (Fig. 33) is a bona fide isochron. In addition, the high percentage (35%) of ordered data further diminishes the possibility of it being an accidental line in a chaotic field.

Assuming the general applicability of the model of Stacey and Kramers (1975) to the evolution of radiogenic terrestrial reservoirs (section 5.3), attempts were made to fit the Iceland isochron to a least-modified version of that model. A near perfect fit is achieved by decreasing the value of μ_1 of the first stage (4.56–3.70 Ga) by 3.4% from 7.19 to 6.945, and decreasing μ_2 of the second stage (3.70 Ga to the present) by 0.2% from 9.74 to 9.72. The result is shown in Figure 33c. The near agreement with the model is in itself not a proof to the validity of the age calculated from the data; the line could still be an

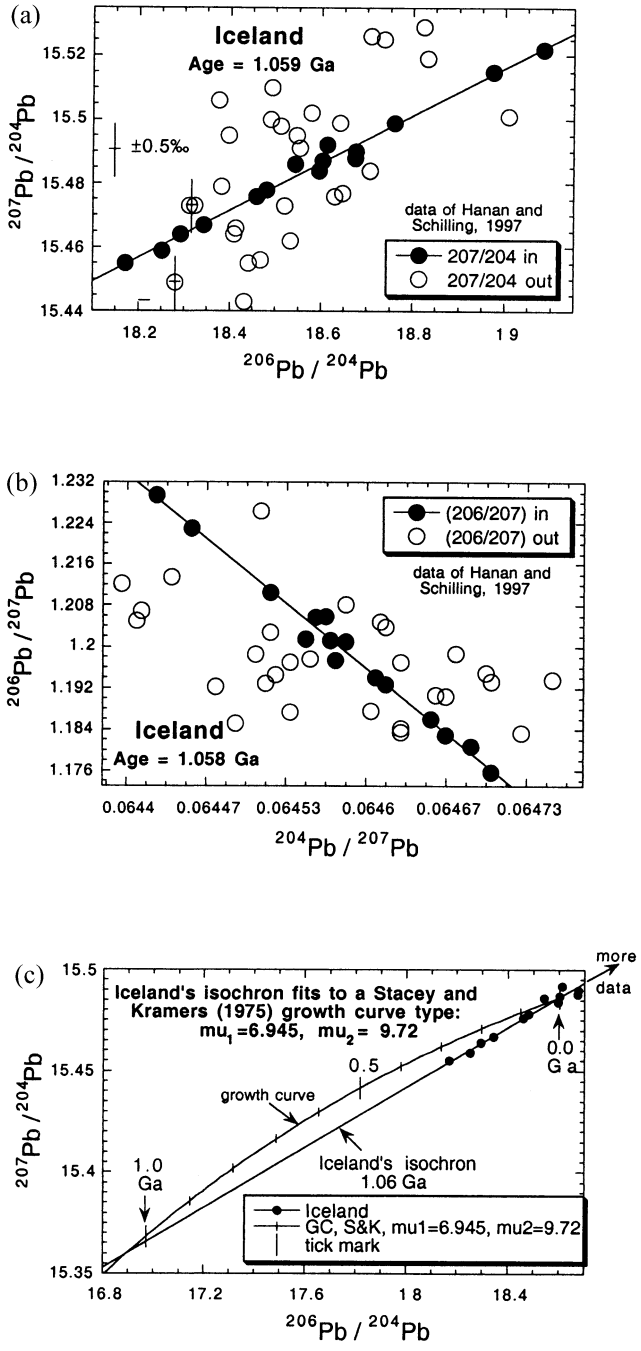

Fig. 33. (a) Age of Iceland lava from type I diagram. (b) The same age is obtained from type III diagram. Compare with age from the unfiltered data on type II diagram (Fig. 31b). (c) The Pb-Pb isochron of Iceland is compatible with the growth curve of a two-stage model with parameters (times and μ values; see text) very close to those of Stacey and Kramers (1975).

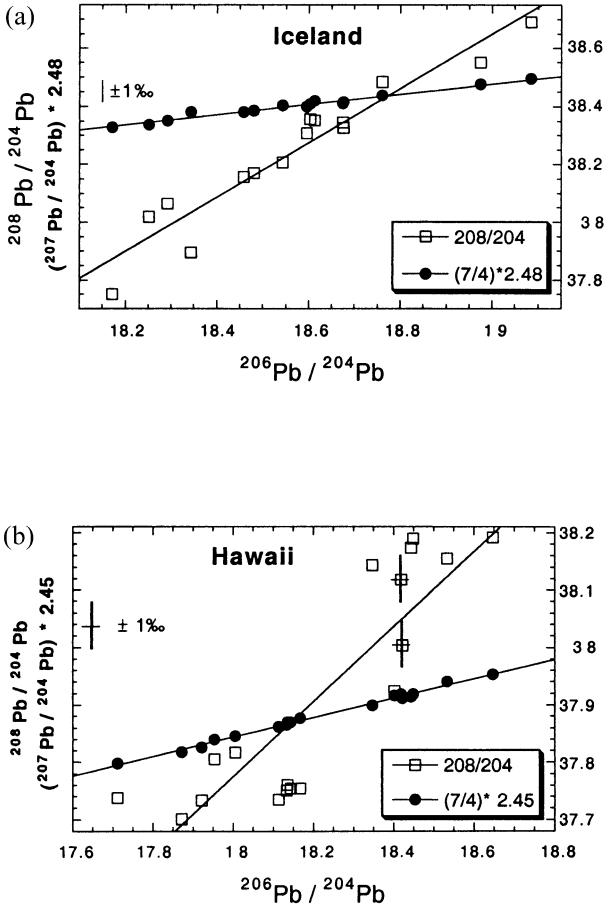

Fig. 34. (a) Iceland: both $^{208}Pb/^{204}Pb$ and $^{207}Pb/^{204}Pb$ ($\times$ 2.48 for convenience) are plotted vs. $^{206}Pb/^{204}Pb$. The coherent linearity of ^{207}Pb is not matched by ^{208}Pb. This seems to preclude the scenario of a mixing line for two homogeneous end-members (see text). (b) Hawaii: both $^{208}Pb/^{204}Pb$ and $^{207}Pb/^{204}Pb$ ($\times$ 2.45 for convenience) are plotted vs. $^{206}Pb/^{204}Pb$. Here too, the disparity between the patterns of ^{208}Pb and ^{207}Pb is apparent, even more pronounced.

artifact. However, the accumulated evidence appears to point to an isochron condition.

Isochronism appears further substantiated on the basis of Figure 34a, where both $^{208}Pb/^{204}Pb$ and $^{207}Pb/^{204}Pb$ ($\times$ 2.48, for convenience) are plotted vs. $^{206}Pb/^{204}Pb$. In contrast to the strong coherence of $^{207}Pb/^{204}Pb$ data, the scatter in $^{208}Pb/^{204}Pb$ data appears to preclude simple mixing between two homogeneous end-members. However, if the evidence of isochron authenticity (mentioned above) is discounted, a mixing line scenario is possible if one of the end-members is allowed to be heterogeneous in $^{208}Pb/^{204}Pb$ (e.g., as a result of long-term varied Th/Pb but uniform U/Pb). This dichotomy is not highly probable. The physical scenario corresponding to isochronism is that of a hot spot tapping a reservoir, which at 1 Ga was homogenized and at about the same time was fractionated in U-Pb on a smaller scale. This fractionation was preserved till (or close to) the present.

5.6.2. An Iceland-Hawaii Isochron?

Similarly, almost exactly the same observations and conclusions could be said about the Hawaiian lavas. Here, 24% of the data on the Hawaiian volcanoes (18 out of 74 points) are found to be synchronous at an age of 0.913 $\pm$ 0.0004 Ga (no figures shown). Perhaps accidentally, this age is in the neighborhood of an age of 0.94 $\pm$ 0.42 Ga based on unfiltered data on the

Hawaiian volcanoes (Tatsumoto, 1978). Similar to Iceland but more pronounced is the contrast between the coherence of $^{207}Pb/^{204}Pb$ and the dispersion of the $^{208}Pb/^{204}Pb$, when plotted against $^{206}Pb/^{204}Pb$ (see Fig. 34b).

Besides the closeness of the ages, the two isochrons (of Iceland and Hawaii) are found to have superposed trajectories, as shown in Figure 35. Unless the observation is an artifact of geometry, the super position of the isochrons suggests initiation of the linear Pb pattern (in each case) from the same initial Pb composition at ~1 Ga ago. The vast geographical separation between Hawaii and Iceland suggests that such an homogenizing event may have been a global thermal episode. Alternatively, both Hawaii and Iceland could have been derived from the same ancient "global" reservoir, which had been homogenized at an earlier (possibly much earlier) global event.

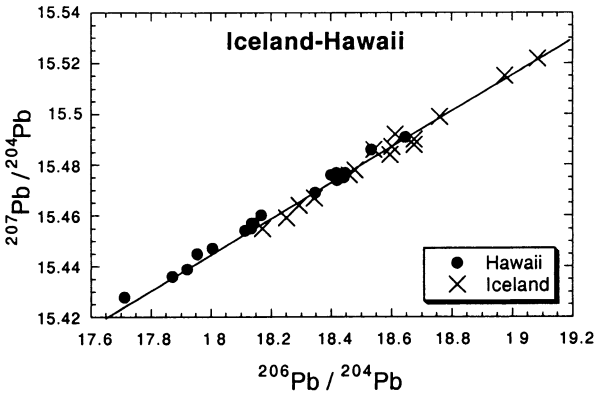

Fig. 35. Filtered Pb data of Hawaii and Iceland appear co-linear. This indicates similarity of initial Pb.

5.6.3. *Cataclysmic Differentiation?*

For either of the above interpretations regarding a single initial Pb for Hawaii and Iceland to be generally valid, two counter processes must be coupled: (1) isotopic homogenization on a macro scale (thousands of kilometers of surface distances) into a single initial Pb (or a single homogeneous reservoir), followed by (2) establishment of wide spread (globe-wide?) fixed elemental U-Pb heterogeneities on a vastly smaller scale (meters to kilometers?), at 1 Ga.

The coupling of two extreme counter effects operating along mammoth dimensions suggests a catastrophic planetary process: perhaps instantaneous "reservoir detonation" and formation of an unstable hydrous "broth," which no sooner it had been isotopically homogenized than it was instantaneously dehydrated, leaving behind ranges of trace element heterogeneity. On the basis of a model discussed in section 4.4, this event could have taken place at 4.55 Ga and again at 3.25 Ga. Subsequent to the 3.25-Ga event, a state of organized convection entailing the slow mobility of coherent large blobs was soon established. Within these blobs, parent-daughter heterogeneity (3.25 Ga old?) is generally preserved. However, this ancient imprint was subject to some modification by the superposition of a milder event (largely within the blobs?) at ~1 Ga.

In this regard two items may be worth mentioning: (1) calculations by Manga (1996) indicate that high-viscosity blobs could survive in convective cells for geologically long times, without substantial deformation or mixing with the surrounding flow. Also, Zindler et al. (1984) argued for a mantle that is heterogeneous on a kilometer or smaller scale; (2) Stein and Hofmann (1994) and Breuer and Spohn (1995) proposed models of catastrophic switching from layered convection to whole-mantle convection, caused by the sudden sinking of accumulated material of descending plates (at the 660-km seismic discontinuity) into the lower mantle.

Other ocean islands with enough filtered data which yield synchronous lines (not shown), are Pitcairn (0.8 Ga, data of Woodhead and Devey, 1993) and Kerguelen and Cape Verde (2.2 and 1.4 Ga, respectively; original references in Zindler and Hart, 1986). If proven to be isochrons, they may indicate repeated fractionation events coupled with long-term preservation of U-Pb heterogeneity in closed-system blobs.

It should be mentioned that the tight Pb-Pb trends for some OIB discussed above, were found not to correlate with $^{87}Sr/^{86}Sr$ or $^{143}Nd/^{144}Nd$ for these samples. Perhaps this should not be surprising because correlation would require stringent behavioral parallelism between the different parent-daughter systems.

5.6.4. *Do Magma Fields Define Spatio-Temporal Planes?*

In Figure 36 are shown the high-precision Pb isotopic data on the Mauna Kea volcano (Abouchami et., al, 2000). By rejecting just 4 data points (out of 29), it is seen that the remaining samples (86%) fall on four well-resolved, well-defined parallel lines. In particular, lines A, B and C have the same slope, and may serve as a verification of a stringently systemic, fine-scale phenomenon. From border to border, the four parallel lines are separated horizontally by a 7‰ range in $^{206}Pb/^{204}Pb$, a measure of the remarkable resolution attained by the original authors (Abouchami et., al., 2000). Irrespective of the eventual final interpretation of these lines, they appear to be the result of a highly constrained phenomenon of replication. One such phenomenon put forward here is translocation-isochronism (see section 4.3), which entails a mechanism possibly applicable to the observation under consideration.

Considering the apparent existence of an 0.9-Ga imprint in

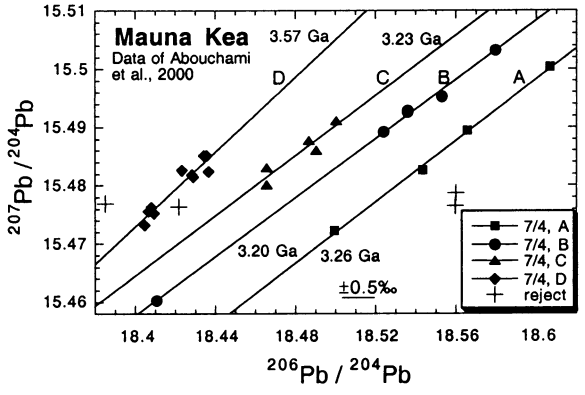

Fig. 36. High-precision Pb data on Mauna Kea seem to reveal a process of line-replication (see section 4 on lineation).

the Hawaiian data (see section 5.6.2), it may be reasonable to assume that the observed translocation was mediated in the Mauna Kea lava during that event. It may also be reasonable to consider the occurrence of line-replication in the Hawaiian lava in general. This possibility first arose from the apparent organization of the Hawaiian Pb data into three clusters (see Fig. 11b). Specifically, I pose the general question: Are the three clusters largely the result of discrete U-Pb fractionation in a mirror-image fashion, where U gain in one group of samples (right cluster) is matched by U loss in another (left cluster)? Implicit in this question is the assumption that the central cluster is the original pattern from which the other two were derived (see chronoplane concept, section 4.4).

On the basis of the Mauna Kea observation (Fig. 36), and a 0.9-Ga isochron for Hawaii (section 5.6.2) a synthetic chronoplane is constructed (Fig. 11a) which is superimposed here on the Hawaiian data (Fig. 37a). Each of the three longitudinal lines of the chronoplane is contained in an envelope that is $\pm 2‰$ wide. It is seen in Figure 37a that $> 70\%$ of the data in the central cluster fall within the borders of the central envelope. For the two outer clusters $> 50\%$ of the data in each case, fall within the borders of each of the two flank-envelopes (Fig. 37a).

Some inconsistency remains, however: the chronoplane outlined (Fig. 11a) was prompted by the apparent replication of a 3.25-Ga line by the Mauna Kea data (Fig. 36). Self-consistency would require the Mauna Kea data to be associated with the 3.25-Ga isochron in Figure 37a. Instead they appear associated with the 3.56-Ga envelope, with expansion farther to the right (Fig. 37b). It should be pointed out in this connection that translocation at a very recent time can cause a big shift associated with a small change in the slope of the shifted isochron. For example, translocation at 0.1 Ga with $\mu = 25$ can shift the 3.25-Ga line in Figure 37b into the center of the Mauna Kea data while changing the age to 3.28 Ga. If valid, this scenario requires that the Mauna Kea lava did not participate in the inferred 0.9-Ga event, but its source experienced strong U enrichment very recently.

In Figure 37c the Iceland data are seen to spread to the right beyond the Hawaiian chronoplane (solid lines). However, increasing μ_3 from 11.3 to 13.3 is enough to expand the parallelogram to enclose most of the Iceland data (see Fig. 37c). It is also possible that Iceland samples experienced additional translocation in a recent event. Some of the data on Iceland by Chauvel and Hémond (2000) fall far outside the expanded chronoplane, indicating a more complex history, or serious interlaboratory bias.

The potential difficulty with Pb isotopic data from different laboratories is dramatically illustrated by the data on the South Sandwich Islands from two laboratories (Cohen and O'Nions, 1982; Barreiro, 1983), where the $^{206}Pb/^{204}Pb$ values for the same samples in the two studies are significantly different (no figure). In addition to such interlaboratory bias one must add a potentially poor control of fractionation, which would further contribute to the creation of artificial scatter. Thus the scatter in OIB data, and the chronoplane of Hawaii, must be considered with reservation. The need for high quality data as in Abouchami et al. (2000) appears more timely than ever.

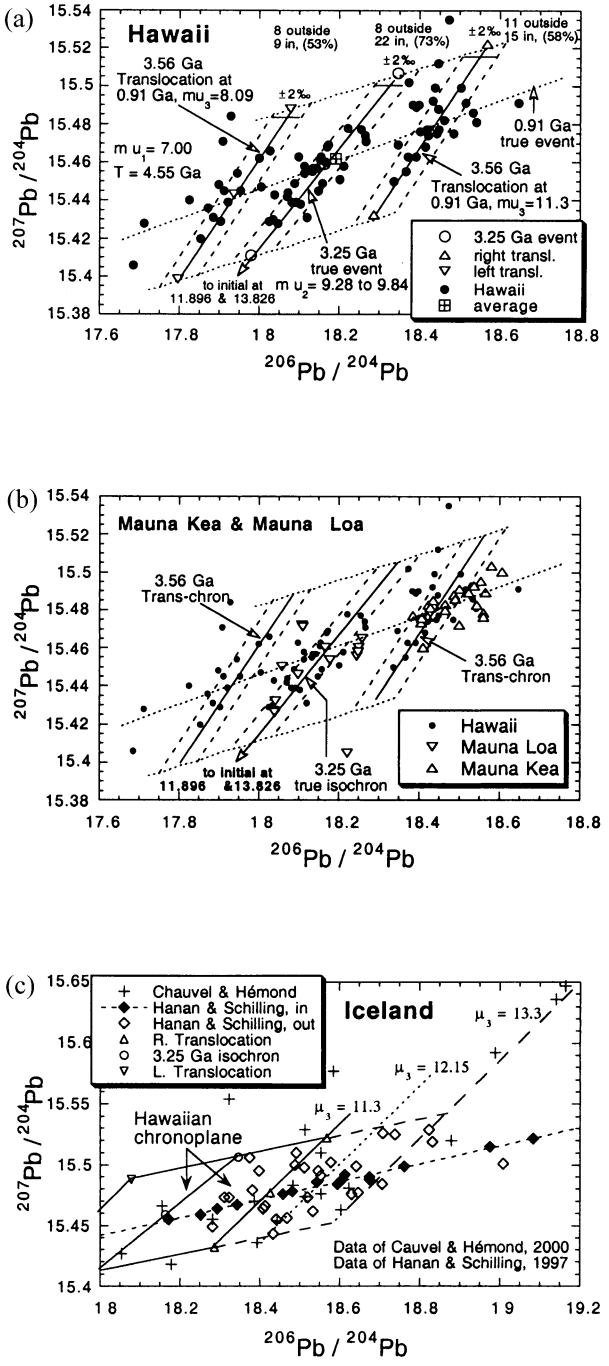

Fig. 37. (a) The synthetic chronoplane of Figure 11a is superimposed here on the Hawaiian data, which appear to be correlated with the model's three envelopes. The central cluster of the data appears associated with the 3.25-Ga isochron, where ~73% of the points fall within the ±2‰ width of the envelope. For the right and left translocation-isochrons, the level of association is on the order of ~58 and ~53%, respectively. Note location of the point of the Hawaiian average close to the intersection of the two true isochrons of the model. (b) Mauna Kea's association appears to be with the right flank translocation-isochron. While line D in Figure 36 is consistent with such association, the three other lines in Figure 36, as well as the overflow of data further to the right in Figure 37b, suggest a more complex evolution. (c) Iceland data points plot mostly to the right of the "Hawaiian chronoplane." In a variation on the theme, the chronoplane is extended to the right to cover the bulk of the Iceland data, by simply raising μ_3 from 11.3 to 13.3. The large $^{207}Pb/^{204}Pb$ scatter in the data of Chauvel and Hémond (2000) is enigmatic.

6. SUMMATION

This text is multi-thematic; thus a brief summation of the main facets of the subject may be in order. For convenience, the manuscript may be divided into three parts:

6.1. Theory: Three Concepts and a Procedure

Accurate dating of disturbed geologic systems using the three Pb isotopes 204, 206, and 207 is not only possible, it is practical. The same three isotopes can be used to construct three equivalent Pb-Pb diagrams. With variable U/Pb, same closed-system data define the same temporal line in each of the diagrams. But same open-system data are generally projected into variably modulated patterns. Thus while the three ages (from the three diagrams) of a closed system are synchronous within a few 10^6 yr, at most, those of an open system can vary by $> 10^7$ yr (see Fig. 1). This dichotomy of age projection is the crux of *Pb isotope synchronism*, which under favorable (but not unusual) conditions can accurately date filtered disturbed systems.

The filtration procedure, *Pb differential correlation*, relies on separately plotting 206/204 and 207/204 vs. the difference between the two ratios, and exploits the contrast. Because ^{206}Pb is produced essentially linearly, while ^{207}Pb in an "avalanche" tailing off since 3 Ga, the correlation of the former is generally a line irrespective of disturbance, while that of the latter is more of a dispersion field. A common x-axis allows tracking the shifts of disturbed data (see Fig. 2). The above differential disparity is used for filtering systems 3.5 Ga and younger. Older systems are identified by differential coincidence, where the two correlations concur in resolving (thus identifying) the older systems (see Figs. 7 and 18).

Two-stage lineation is the result of a disturbance characterized by the uniformity of either μ_3 (that is ^{238}U/^{204}Pb in the third stage) or F (where $F = \mu_3/\mu_2$). Lines resulting from a singular F are termed *transposition-isochrons* (Fig. 9); and those affected by constant μ_3 are called *translocation-isochrons* or simply *trans-chrons* (Fig. 10a). Irrespective of the value of constant μ_3, a trans-chron appears always "older" than the true age of the undisturbed samples. Furthermore, trans-chrons (resulting from a series of constant μ_3) of a given event, form a series of lines (of the same "age") that run parallel to each other; that is, the slope of a trans-chron is dependent only on the time of the disturbance. In contrast, the slope of a transposition-isochron is dependent on the value of F as well. $F < 1$ delays isotopic evolution, giving rise to a retarded (that is, "older") isochron, while $F > 1$ leads to an accelerated ("younger") isochron. Interestingly, irrespective of whether accelerated or retarded, transposition-lines of a given parent isochron converge on each other and intersect in a single point. That point of intersection is the actual initial Pb of the system (Fig. 9b).

The formation of a *chronoplane* (Fig. 11a) may be affected through the superposition of a special form of disturbance (bipolar) within a contained system (S), where the creation of a domain with a constant μ_3 that is $>\mu_s$ is attained on the expense of a uniform depletion in another domain with $\mu_3 < \mu_s$. As a result, two parallel trans-chrons are formed, defining the longitudinal borders of a chronoplane. Assuming symmetrical U-Pb fractionation in the predisturbance stage (partly due to the containment of the system), the highest and lowest ^{207}Pb/^{204}Pb values of the undisturbed samples (of a thoroughly sampled system) would define the width of the chronoplane. The isochron yielding the age of the disturbance is defined by samples which fractionated in the disturbance, but escaped fractionation in the prior event.

6.2. Observation

1. A synchronous Pb-Pb line yielding a 4.42-Ga age for some of the Amîtsoq rocks (Figs. 18 and 19).
2. Isochrons of some rocks intersect at a point less evolved than "modern terrestrial Pb" (Figs. 22 and 23).
3. Ordinary chondrites define a single, highly synchronous Pb-Pb line, from which a 4.555-Ga age is calculated (Fig. 29).
4. Preservation of ~1-Ga synchronous line in the filtered data of both Iceland and Hawaii (Figs. 32, 33, and 35).
5. High precision Pb-Pb data on the Mauna Kea volcano fall on four parallel lines (Fig. 36).
6. Apparent organization of the Hawaiian Pb-Pb data in three "parallel" clusters (Figs. 11b and 37a).

6.3. Interpretation

1. The 4.42-Ga line is given two possible explanations: (1) it is an artifact, specifically a translocation-isochron, resulting from a 2-Ga disturbance in a 3.73-Ga system. (2) It is a true isochron, indicating the survival of some vestiges of an ancient crust. It is argued that tenuous evidence for that ancient imprint appear to exist in some old zircons (Figs. 24–28).
2. The point of intersection of some filtered isochrons is tentatively interpreted as a present-day Pb composition of a U-depleted source. If valid the result may represent a (partial?) solution to the "Pb paradox."
3. Ordinary chondrites belong to a single parent body that is 4.555 Ga old.
4. Iceland and Hawaii experienced a 1-Ga event, from which a single initial Pb is inferred. This would seem to necessitate episodic "global" homogenization.
5. Mauna Kea lava is imprinted by a fine-scale, line-replicating mechanism, superimposed on ~3.25-Ga event. This could be affected by translocation-isochronism in recent times.
6. The Hawaiian parallel trends may be explained as aspects of a chronoplane caused by the superposition of an 0.9-Ga event on an ~ 3.25-Ga system. As such they suggest operational line-replication (translocation-isochronism) on a large scale. However, in view of evidence to the existence of gross interlaboratory bias (in other data), one must consider the Hawaiian pattern with reservation.

Acknowledgments—I benefited from criticism and comments by Stephen J. G. Galer, G. J. Wasserburg, and an anonymous reviewer. Their remarks prompted elaboration which I hope elucidated the issues. I am also grateful to the associate editor, Steven L. Goldstein, for suggestions which improved the manuscript and expanded its range. The subsequent beneficial involvement of the executive editor, Frank A. Podosek, is gratefully acknowledged. I thank Merri Wolf (of DTM Library Staff) for kindly proof-reading this manuscript.

Associate editor: S. L. Goldstein

REFERENCES

Abouchami W., Galer S. J. G., and Hofmann A. W. (2000) High precision lead isotope systematics of lavas from the Hawaiian Scientific Drilling Project. *Chem. Geol.* **169,** 187–209.

Barreiro B. (1983) Lead isotopic composition of South Sandwich Island volcanic rocks and their bearing on magmagenesis in intra-oceanic island arcs. *Geochim. Cosmochim. Acta* **47,** 817–822.

Black L. P., Moorbath S., Pankhurst R. J., and Windley B. F. (1973) $^{207}Pb/^{206}Pb$ whole rock ages of the archaean granulite facies metamorphic event in West Greenland. *Nature* **244,** 50–53.

Black L. P., Williams I. S., and Compston W. (1986) Four zircon ages from one rock: the history of a 3930 Ma-old granulite from Mount Sones, Enderby Land, Antarctica. *Contrib. Mineral. Petrol.* **94,** 427–437.

Bowring S. A. and Housh T. (1995) The earth's early evolution. *Science* **269,** 1535–1540.

Bowring S. A. and Williams I. S. (1999) Priscoan (4.00-4.03 Ga) orthogneisses from northwestern Canada. *Contrib. Mineral. Petrol.* **134,** 3–16.

Bowring S. A., Williams I. S., and Compston W. (1989) 3.96 Ga gneisses from the Slave province, Northwest Territories, Canada. *Geology* **17,** 971–975.

Breuer D. and Spohn T. (1995) Possible flush instability in the mantle convection at the Archean-Proterozoic transition. *Nature* **378,** 608–610.

Brooks C., Hart S. R., Hofmann A., and James D. E. (1976) Rb-Sr mantle isochrons from oceanic regions. *Earth Planet. Sci. Lett.* **32,** 51–61.

Chapman H. J. and Moorbath S. (1977) Lead isotope measurements from the oldest recognized Lewisian gneisses of north-west Scotland. *Nature* **268,** 41–42.

Chase C. G. (1981) Oceanic island Pb: Two-stage histories and mantle evolution. *Earth Planet. Sci. Lett.* **52,** 277–284.

Chauvel C., Hémond C. (2000) Melting of a complete section of recycled oceanic crust: Trace element and Pb isotopic evidence from Iceland. *Geochem. Geophys. Geosys.* **1,** paper #1999GC0 00002.

Chen J. H. and Wasserburg G. J. (1981) The isotopic composition of uranium and lead in Allende inclusions and meteoritic phosphates. *Earth Planet. Sci. Lett.* **52,** 1–15.

Cohen R. S. and O'Nions R. K. (1982) Identification of recycled continental material in the mantle from Sr, Nd and Pb isotope investigations. *Earth Planet. Sci. Lett.* **61,** 73–84.

Compston W. and Pidgeon R. T. (1986) Jack Hills, evidence of more very old detrital zircons in Western Australia. *Nature* **321,** 766–769.

Froude D. O., Ireland T. R., Kinny P. D., Williams I. S., Compston W., Williams I. R., and Myers J. S. (1983) Ion microprobe identification of 41000-42000 Myr old terrestrial zircons. *Nature* **304,** 616–6185927.

Göpel C., Manhes G., and Allègre C. J. (1994) U-Pb systematics of phosphates from equilibrated ordinary chondrites. *Earth Planet. Sci. Lett.* **121,** 153–171.

Goldstein S. L. and Galer S. J. G. (1992) On the trail of early mantle differentiation; $^{142}Nd/^{144}Nd$ ratios of early archean rocks. *Eos: Trans. Am. Geophys. Union* **73,** 323.

Hanan B. B. and Schilling J.-G. (1997) The dynamic evolution of the Iceland mantle plume: The lead isotope perspective. *Earth Planet. Sci. Lett.* **151,** 43–60.

Harper C. L. and Jacobsen S. B. (1992a) Evidence from coupled ^{147}Sm-^{143}Nd and ^{146}Sm-^{142}Nd systematics for very early (4.5 Ga) differentiation of the Earth's mantle. *Nature* **360,** 728–732.

Harper C. L., Jacobsen S. B (1992b) $^{146,147}Sm$-$^{142,143}Nd$ systematics of early terrestrial differentiation. In *Proc. Lunar Planet. Sci. Conf. XXIII*, p. 487. Pergamon, New York.

Hart R. J., Welke H. J., and Nicolaysen L. O. (1981) Geochronology of the deep profile through archean basement at Vredefort, with implications for early crustal evolution. *J. Geophys. Res.* **86,** 10663–10680.

Hart R. S. (1984) A large-scale isotope anomaly in the Southern Hemisphere mantle. *Nature* **309,** 753–757.

Kamber B. S. and Moorbath S. (1998) Initial Pb of the Amîtsoq gneiss revisited: Implication for the timing of early Archaean crustal evolution in West Greenland. *Chem. Geol.* **150,** 19–41.

Ludwig K. R. (2001) *Users Manual for Isoplot/Ex v. 2.49: A Geochronological Toolkit for Microsoft Excel*. Berkeley Geochronology Center Special Publication No. 1a.

Lugmair G. W. and Galer S. J. G. (1992) Age and isotopic relationships among the angrites Lewis Cliff 86010 and Angra dos Reis. *Geochim. Cosmochim. Acta* **56,** 1673–1694.

Manga M. (1996) Mixing of heterogeneities in the mantle: Effect of viscosity differences. *Geophys. Res. Lett.* **23,** 403–4064.

Murakami T., Chakoumas B. C., Ewing R. C., Lumpkin G. R., and Weber W. J. (1991) Alpha-decay event damage in zircon. *Am. Mineral.* **76,** 1510–1532.

Nasdala L., Pidgeon R. T., and Wolf D. (1996) Heterogeneous metamictization of zircon on a microscale. *Geochim. Cosmochim. Acta* **60,** 1091–1097.

Nutman A. P., McGregor V. R., Friend C. R. L., Bennett V. C., and Kinny P. D. (1996) The Itsaq gneiss complex of southern West Greenland; the world's most extensive record of early crustal evolution. *Precam. Res.* **78,** 1–39.

Nutman A. P., Bennett V. C., Friend C. R. L., and McGregor V. R. (2000) The early archaean Itsaq gneiss complex of southern Western Greenland: The importance of field observations in interpreting age and isotopic constraints for early terrestrial evolution. *Geochim. Cosmochim. Acta* **64,** 3035–3060.

Patterson C. (1956) Age of meteorites and the earth. *Geochim. Cosmochim. Acta* **10,** 230–237.

Pidgeon R. T., O'Neil J. R., and Silver L. T. (1966) Uranium and lead isotopic stability in a metamict zircon under experimental hydrothermal conditions. *Science* **154,** 1538–1540.

Reynolds P. H. (1971) A U-Th-Pb isotope study of rocks from Broken Hill, Australia. *Earth Planet. Sci. Lett.* **12,** 215–223.

Sharma M., Papanastassiou D. P., Wasserburg G. J., and Dymek R. F. (1996) The issue of terrestrial record of ^{146}Sm. *Geochim. Cosmochim. Acta* **60,** 2037–2047.

Stacey J. S. and Kramers J. D. (1975) Approximation of terrestrial lead isotope evolution by a two-stage model. *Earth Planet. Sci. Lett.* **26,** 207–221.

Stein M. and Hofmann A. W. (1994) Mantle plumes and episodic crustal growth. *Nature* **372,** 63–68.

Sun S. S. and Hanson G. N. (1975) Evolution of the mantle: Geochemical evidence from alkali basalt. *Geology* **3,** 297–302.

Tatsumoto M. (1978) Isotopic composition of lead in oceanic basalt and its implication to mantle evolution. *Earth Planet. Sci. Lett.* **38,** 63–87.

Tatsumoto M., Knight J. K., and Allègre C. J. (1973) Time differences in the formation of meteorites as determined from the ratio of lead-207 to lead-206. *Science* **180,** 1279–1283.

Taylor P. N. (1975) An early precambrian age for migmatitic gneisses from Vikan I BO, Vetsteralen, North Norway. *Earth Planet. Sci. Lett.* **27,** 35–42.

Tera F. (1983) U-Th-Pb in chondrites. Evidence to elemental mobilities and the singularity of primordial Pb. *Earth Planet. Sci. Lett.* **63,** 147–165.

Tera F. (2000a) Lead isotope synchronism and the search for the earth's ancient crust [abstract]. *Lunar Planet. Sci. Conf.* **31**..

Tera F. (2000b) Inference from the lead isotopes to the survival of a terrestrial crust 4.4 Ga old [abstract]. *AGU Spring Meeting V22B.*

Tera F. and Wasserbug G. J. (1972a) U-Th-Pb systematics in lunar highland samples from Luna 20 and Apollo 16 missions. *Earth Planet. Sci. Lett.* **17,** 36–51.

Tera F. and Wasserbug G. J. (1972b) U-Th-Pb systematics in three Apollo 14 basalts and the problem of initial Pb in lunar rocks. *Earth Planet. Sci. Lett.* **14,** 281–304.

Tera F. and Carlson R. W. (1999) Assessment of the Pb-Pb and U-Pb chronometry of the early solar system. *Geochim. Cosmochim. Acta* **63,** 1877–1889.

Tera F., Papanastassiou D. A., and Wasserburg G. J. (1974) Isotopic evidence for a terminal lunar cataclysm. *Earth Planet. Sci. Lett.* **1,** 1–21.

Tera F., Carlson R. W., and Boctor N. Z. (1997) Radiometric ages of basaltic achondrites and their relation to the early history of the Solar System. *Geochim. Cosmochim. Acta* **63,** 1713–1731.

Unruh D. M. (1982) The U-Th-Pb age of equilibrated L chondrites and a solution to the excess radiogenic Pb problem in chondrites. *Earth Planet. Sci. Lett.* **58,** 75–94.

Williams I. S., Compston W., Black L. P., Ireland T. R., and Foster J. J. (1984) Unsupported radiogenic Pb in zircon: A cause of anomalously high Pb-Pb, U-Pb and Th-Pb ages. *Contrib. Mineral. Petrol.* **88,** 322–327.

Wilde S. A., Valley J. W., Peck W. H., and Graham C. M. (2001) Evidence from detrital zircons for the existence of continental crust and oceans of the earth 4.4 Ga ago. *Nature* **409,** 175–178.

Wooden J. L. and Mueller P. A. (1988) Pb, Sr, and Nd isotopic composition of a suite of Late Archean, igneous rocks, eastern Beartooth Mountains: Implications for crust-mantle evolution. *Earth Planet. Sci. Lett.* **87,** 59–72.

Woodhead J. D. and Devey C. W. (1993) Geochemistry of the Pitcairn seamounts, I: source character and temporal trends. *Earth Planet. Sci. Lett.* **116,** 81–99.

Zindler A. and Hart S. (1986) Chemical geodynamics. *Ann. Rev. Earth Planet. Sci.* **14,** 493–571.

Zindler A., Staudigel H., and Batiza R. (1984) Isotope and trace element geochemistry of young Pacific seamounts: Implications for the scale of upper mantle heterogeneity. *Earth Planet. Sci. Lett.* **70,** 175–195.